Macromolecules

Article

Cite This: Macromolecules XXXX, XXX, XXX–XXX

How Does the Hydrogen Bonding Interaction Influence the Properties of Polybenzoxazine? An Experimental Study Combined with Computer Simulation

Xiaobin Shen,[†,‡] Lijun Cao,[†,‡,#] Yuan Liu,[†,‡] Jinyue Dai,[†,‡] Xiaoqing Liu,[*,†,§] Jin Zhu,[†,§] and Shiyu Du[†]

[†]Ningbo Institute of Materials Technology and Engineering, Chinese Academy of Sciences, Ningbo, Zhejiang 315201, P. R. China

[‡]University of Chinese Academy of Sciences, Beijing 100049, P. R. China

[§]Key Laboratory of Bio-based Polymeric Materials Technology and Application of Zhejiang Province, Ningbo, Zhejiang 315201, P. R. China

Supporting Information

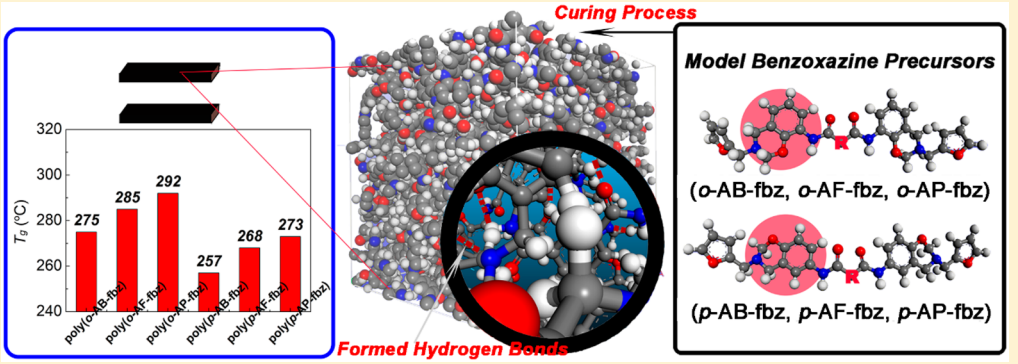

ABSTRACT: The formation of intra- or intermolecular hydrogen bonding and their influences on polybenzoxazine's properties were investigated after the model benzoxazine monomers (*o*-AB-fbz, *o*-AF-fbz, *o*-AP-fbz, *p*-AB-fbz, *p*-AF-fbz, *p*-AP-fbz) were synthesized. Because of the different electron-donating abilities of bridging units (benzene, furan and pyridine) in isophthalic acid (IPA), 2,5-furandicarboxylic acid (2,5-FDCA) and 2,6-pyridinedicarboxylic acid (2,6-PDCA), the strength of intramolecular H-bonding involved with the oxygen atom in oxazine ring in *o*-AB-fbz, *o*-AF-fbz and *o*-AP-fbz followed the order of *o*-AB-fbz > *o*-AF-fbz > *o*-AP-fbz, and the strength of the overall H-bonding was arranged as follows: *o*-AB-fbz < *o*-AF-fbz < *o*-AP-fbz. While more intermolecular H-bonding was formed in *p*-AB-fbz and *p*-AF-fbz as well as *p*-AP-fbz. DSC and FT-IR results discovered the relationship between the H-bonding involved with the oxygen atom in oxazine ring and the curing activities of benzoxazines. After curing reaction, the cured systems showed varied glass transition temperature (T_g), and the influence of H-bonding on T_g was revealed by in situ FT-IR analysis. Molecular dynamics (MD) simulation was also applied to investigate the properties of synthesized polybenzoxazines and similar results were obtained. Not only the formation of H-bonding but also their effects on both the curing behaviors of benzoxazine monomers and the thermal properties of cured resins were systematically investigated, which would help us understand polybenzoxazines more deeply and might be a guideline for improving their comprehensive properties only by manipulating the H-bonding.

INTRODUCTION

Polybenzoxazine is a relatively new phenolic-type thermosetting resin that possess a set of desirable properties, including excellent mechanical and electrical properties, low moisture absorption, high chemical and thermal resistance and low flammability.[1,2] In addition, its precursor, benzoxazine can be synthesized from various phenols, amines and formaldehyde via the Mannich condensation reaction, which ensures its rich molecular design flexibility.[3] As for the curing reaction, no hardeners or catalysts is needed and nearly no byproducts or toxic volatiles are generated.[4] All of these advantages have made polybenzoxazine to attract more and more attention from both industry and academic communities in recent years, leading to wide applications in the field of electronic packaging, aerospace and transportation et al.[5,6]

However, the properties of polybenzoxazines, especially their high brittleness, low cross-link density, and high curing temperature, are still subjects to be improved in order to meet the varied application requirements. Over the past two decades, numerous efforts have been made to develop the new

Received: April 6, 2018
Revised: June 18, 2018

DOI: 10.1021/acs.macromol.8b00741
Macromolecules XXXX, XXX, XXX–XXX

Scheme 1. Chemical Structures of Model Benzoxazine Monomers Containing Amide Groups at *ortho*- and *para*-Positions with Respect to the Oxygen Atom (*o*-AB-fbz, *o*-AF-fbz, *o*-AP-fbz, *p*-AB-fbz, *p*-AF-fbz, and *p*-AP-fbz)

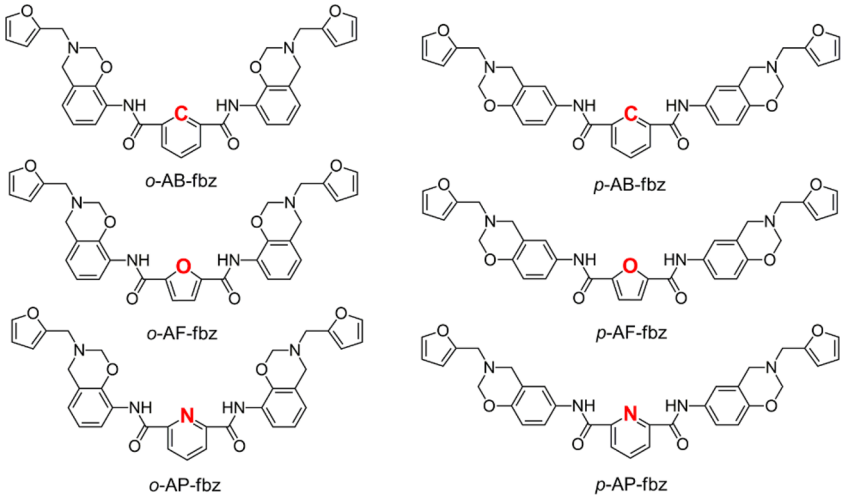

polybenzoxazine systems with enhanced or satisfied properties.[7−25] And the general strategies can be cataloged into (1) blending or alloying benzoxazines with other polymers,[7−11] (2) reinforcing polybenzoxazines with fibers[12−15] or inorganic particles,[16−18] (3) functionalizing benzoxazine monomers with additional reactive groups,[19−23] and (4) synthesizing main chain or side chain polybenzoxazine precursors.[24,25] On the basis of these works, it could summarize that the features of polybenzoxazines are mainly attributed to the chemical structures of benzoxazine monomers and the formation of Mannich based bridges as well as the inter- and intramolecular H-bonding in the networks after curing reaction.[26,27]

Recently, Ishida and his co-workers[28−30] investigated the catalytic effect of H-bonding involved with the oxygen atom in oxazine ring and the *o*-methylol/amide groups. They found that the H-bonding could accelerate the initiation of polymerization and slow down the chain propagation. Especially, the intramolecular five-membered H-bonding between *o*-amide group (−CON*H*−) and oxazine ring (−Ar*O*CH$_2$−) could act like a self-complementary initiator, which reduced the curing temperature of *o*-amide benzoxazine by 60 °C.[28] The intramolecular interaction between aromatic hydrogen and oxazine ring, which was responsible for the curing temperature differences between *ortho*-, *meta*- and *para*-positioned bis(benzoxazine)s, was also reported in Endo's work.[31] Moreover, the H-bonding interaction was also employed for the property enhancement of polybenzoxazines.[32−36] For example, Yagci et al.[32,33] prepared several kinds of self-healing polybenzoxazines taking advantage of inter- or intramolecular hydrogen bonding in the cured network. Qutubuddin and his co-workers[34] prepared chitosan/polybenzoxazine cross-linked films with improved thermal and mechanical properties, and the H-bonding might play a crucial role. Most recently, the higher glass transition temperature (T_g) of furan-based polybenzoxazine was attributed the more H-bonding interaction between the oxygen atom in furan ring and Ar-*OH*, when compared with the polybenzoxazine derived from diaminodiphenylmethane (DDM).[35] And the increased surface free energy of main-chain type polybenzoxazine synthesized from different aromatic diamines was also attributed to the increased intermolecular H-bonding in Lin's work.[36] Undoubtedly, H-bonding plays a significant role in determining not only the polymerization temperature and rate of benzoxazine monomers, but also the thermal and mechanical properties as well as other unique features of cured resins. Therefore, the systematical experimental or theoretical insight into the formation of H-bonding and its effect on the comprehensive properties of cured resins is a very essential for polybenzoxazine research.

However, due to the complicated polymerization mechanism of benzoxazines and the complex chemical structures of cured resins,[28,31,37,38] the investigation on the formation or behaviors of H-bonding in benzoxazine is far from enough, especially for the cured systems. Sometimes, the hypothesis or reasoning was more than experimental evidence. As mentioned above, Ishida et al.[27,29,30] conducted some pioneer works on the scientific evidence of H-bonding formation in benzoxazine monomers. With the help of FT-IR[39−42] and NMR,[43−45] the formation of intra- and intermolecular H-bonding in benzoxazine monomers was identified and their influence on the polymerization initiation were reported. However, because of the experimental limitation, the strength of H-bonding interaction and its relationship to the curing reactivity of benzoxazines were not investigated yet. And what we should emphasize was that, the experimental evidence about the relationship between H-bonding strength and thermal properties of polybenzoxazine networks was rarely reported in literatures.

Hence, in order to obtain deeper and more fundamental understanding about the formation and strength of H-bonding in polybenzoxazine, the model benzoxazine monomers, containing amide groups at *ortho*- or *para*-position with respect to the oxygen atom in oxazine ring, were carefully designed and synthesized from isophthalic acid (IPA), 2,5-furandicarboxylic acid (2,5-FDCA) and 2,6-pyridinedicarboxylic acid (2,6-PDCA) (Scheme 1). It was easy to notice that the bridging units (benzene, furan and pyridine) in the benzoxazines possessed different electron-donating abilities (different basicity), which could tailor or manipulate the strength of H-bonding interaction between the amide group (−CON*H*−) with other electron-donating groups, such as −Ar*O*CH$_2$− and Ar−*O*H. On the basis of which, not only the formation of H-bonding, but also their strength could be characterized and qualitatively compared. Therefore, the effect

DOI: 10.1021/acs.macromol.8b00741
Macromolecules XXXX, XXX, XXX−XXX

of H-bonding strength on the thermal properties of polybenzoxazine could be experimentally investigated. We believe that the information provided in this paper would help us understand polybenzoxazine more deeply.

Furthermore, molecular dynamics (MD) simulation is becoming increasingly important for the study of polymeric materials, as it provides a method to numerically confirm the theoretical models, which help us intuitively observe the structures of polymers in "molecular size". As we know, the early models for cross-linked networks have been created through static algorithms[46] and stepwise algorithms[47−51] during the cross-linking reaction. And most recently, MD simulations have been already tried to investigate the microstructural properties of polybenzoxazines.[52,53] In this work, the MD simulation was also employed to study the formation of H-bonding in the model polybenzoaxzines and predict their properties, which was an useful tool to verify the experimentally observed properties.

EXPERIMENTAL SECTION

Materials. Chemicals and solvents used in this work were purchased from Aladdin Reagent, China, including isophthalic acid (IPA) (99%), 2,6-pyridinedicarboxylic acid (2,6-PDCA) (99%), *o*-aminophenol (98%), *p*-aminophenol (98%), trimethylamine (99%), furfurylamine (FA) (99%), formaldehyde solution (37 wt % in H_2O), sulfoxide chloride ($SOCl_2$) (99%), dimethylformamide (DMF) (99.5%), dimethylacetamide (DMAc) (99%), 1,4-dioxane (99%), sodium hydroxide (NaOH) (98%) and chloroform (99%), except 2,5-furandicarboxylic acid (2,5-FDCA) (98%) that was purchased from Chem target Technologies Co., Ltd. (Mianyang China). All the chemicals were used as received.

Synthesis of Monomers. *2,5-Furandicarbonyl Dichloride (2,5-FDCC).* 2,5-FDCC was obtained following the method described in the previous literature.[54] A mixture containing 11.44 g of 2,5-FDCA (73.4 mmol), 24 mL of $SOCl_2$ (338 mmol), and 200 μL of dimethylformamide (DMF) was refluxed at 80 °C for 4 h with constant stirring. The exhaust should be collected with a concentrated sodium hydroxide aqueous solution through a glass tube from condenser to a washing bottle, packed with activated silica gel. After the excess of $SOCl_2$ and DMF was removed under vacuum at room temperature, the product was isolated and purified by vacuum sublimation to get the white crystal (yield: 76%).

^{1}H NMR (400 MHz, $CDCl_3$, δ, ppm): 7.54 (s, 2H).

1,3-Benzenedicarbonyl Dichloride (1,3-BDCC). 1,3-BDCC was obtained with the similar method to 2,5-FDCC. 12.33 g of IPA (74.2 mmol) was used for 1,3-BDCC. Then white crystal was obtained after purification (yield: 81%).

^{1}H NMR (400 MHz, DMSO-d_6, δ, ppm): 8.47 (s, 1H), 8.14 (dd, J = 7.8, 1.4 Hz, 2H), 7.60 (t, J = 7.7 Hz, 1H).

2,6-Pyridinedicarbonyl dichloride (2,6-PDCC). 2,6-PDCC was obtained with the similar method to 2,5-FDCC. 13.58 g of 2,6-PDCA (81.3 mmol) was used for 2,6-PDCC. Then white crystal was obtained after purification (yield: 70%).

^{1}H NMR (400 MHz, DMSO-d_6, δ, ppm): 8.30 (m, 2H), 8.24 (t, J = 7.6 Hz, 1H).

N2,N5-Bis(2-hydroxyphenyl)furan-2,5-dicarboxamide (Compound 1). Compound **1** was synthesized by reacting *o*-aminophenol with 2,5-FDCC and triethylamine in DMAc.[55] *o*-Aminophenol (9.13 g, 83.6 mmol) was mixed with triethylamine (15.5 mL, 111.6 mmol) in 100 mL of DMAc. Then 2,5-FDCC (5.38 g, 27.9 mmol) dissolved in 50 mL of DMAc was added drop by drop into the mixture. After that the solution was cooled down to 0 °C and kept at this temperature for 4 h, the reaction mixture was poured into cold water and the yellow precipitate was collected via filtration. Finally, it was heated at 50 °C for 8 h in the vacuum oven and the target product was obtained (yield: 84%).

Anal. Calcd for $C_{18}H_{14}N_2O_5$: C, 63.90; H, 4.17; O, 23.65; N, 8.28. Found: C, 64.13; H, 4.21; O, 23.43; N, 8.11.

^{1}H NMR (400 MHz, DMSO-d_6, δ, ppm): 9.87 (s, 2H), 9.73 (s, 2H), 7.69−7.53 (m, 2H), 7.38 (s, 2H), 7.13(m, 2H), 6.96 (d, J = 7.9 Hz, 2H), 6.85 (t, J = 7.3 Hz, 2H).

^{13}C NMR (400 MHz, DMSO-d_6, δ, ppm): 155.87 (s), 150.20 (s), 148.50 (s), 126.59 (s), 125.35 (s), 124.53 (s), 119.21 (s), 116.04 (s).

N1,N3-Bis(2-hydroxyphenyl)isophthalamide (Compound 2). Compound **2** was obtained through a method similar to that used for compound **1**, except that 1,3-BDCC (5.89 g, 29.0 mmol) was taken to replace 2,5-FDCC (yield: 88%).

Anal. Calcd for $C_{20}H_{16}N_2O_4$: C, 68.96; H, 4.63; O, 18.37; N, 8.04. Found: C, 69.09; H, 4.50; O, 18.47; N, 7.97.

^{1}H NMR (400 MHz, DMSO-d_6, δ, ppm): 9.74 (d, J = 17.8 Hz, 4H), 8.58 (s, 1H), 8.17 (d, J = 7.6 Hz, 2H), 7.69 (t, J = 6.6 Hz, 3H), 7.07 (t, J = 7.6 Hz, 2H), 6.99−6.90 (m, 2H), 6.86 (t, J = 7.5 Hz, 2H).

^{13}C NMR (400 MHz, DMSO-d_6, δ, ppm): 165.06 (s), 149.91 (s), 134.93 (s), 130.86 (s), 129.02 (s), 127.00 (s), 126.20 (s), 125.86 (s), 124.89 (s), 119.26 (s), 116.27 (s).

N2,N6-Bis(2-hydroxyphenyl)pyridine-2,6-dicarboxamide (Compound 3). Compound **3** was synthesized through a method similar to that used for compound **1**, except that 2,6-PDCC (5.75 g, 28.2 mmol) was taken to replace 2,5-FDCC (yield: 85%).

Anal. Calcd for $C_{19}H_{15}N_3O_4$: C, 65.32; H, 4.33; O, 18.32; N, 12.03. Found: C, 65.23; H, 4.24; O, 18.43; N, 12.11.

^{1}H NMR (400 MHz, DMSO-d_6, δ, ppm): 10.44 (s, 2H), 10.06 (s, 2H), 8.43−8.38 (m, 2H), 8.33 (dd, J = 8.6, 6.7 Hz, 1H), 8.05 (dd, J = 7.9, 1.3 Hz, 2H), 7.10−7.01 (m, 2H), 6.99 (dd, J = 7.9, 1.0 Hz, 2H), 6.92−6.86 (m, 2H).

^{13}C NMR (400 MHz, DMSO-d_6, δ, ppm): 161.49 (s), 149.33 (s), 148.99 (s), 140.75 (s), 125.90 (d, J = 6.1 Hz), 125.48 (s), 122.60 (s), 119.61 (s), 115.84 (s).

N2,N5-Bis(4-hydroxyphenyl)furan-2,5-dicarboxamide (Compound 4). Compound **4** was obtained by 2,5-FDCC (5.23 g, 27.1 mmol) reacted with *p*-aminophenol (8.86 g, 81.3 mmol) companied with triethylamine (15.1 mL, 108.4 mmol), following a method similar to that used for compound **1** (yield: 89%).

Anal. Calcd for $C_{18}H_{14}N_2O_5$: C, 63.90; H, 4.17; O, 23.65; N, 8.28. Found: C, 64.07; H, 4.28; O, 23.63; N, 8.08.

^{1}H NMR (400 MHz, DMSO-d_6, δ, ppm): 10.11 (s, 2H), 9.44 (s, 2H), 7.50 (t, J = 13.1 Hz, 4H), 7.35 (d, J = 10.0 Hz, 2H), 6.80 (t, J = 9.0 Hz, 4H).

^{13}C NMR (400 MHz, DMSO-d_6, δ, ppm): 155.26 (s), 154.40 (s), 148.32 (s), 129.19 (s), 122.86 (s), 115.84 (s), 115.38 (s).

N1,N3-Bis(4-hydroxyphenyl)isophthalamide (Compound 5). Compound **5** was synthesized from 1,3-BDCC (5.96 g, 29.4 mmol) according to a method similar to that used for compound **4** (yield: 91%).

Anal. Calcd for $C_{20}H_{16}N_2O_4$: C, 68.96; H, 4.63; O, 18.37; N, 8.04. Found: C, 69.13; H, 4.51; O, 18.43; N, 8.01.

^{1}H NMR (400 MHz, DMSO-d_6, δ, ppm): 10.21 (s, 2H), 9.30 (s, 2H), 8.48 (s, 2H), 8.15−8.03 (m, 2H), 7.72−7.60 (m, 2H), 7.56 (d, J = 8.8 Hz, 4H), 6.77 (d, J = 8.8 Hz, 4H).

^{13}C NMR (400 MHz, DMSO-d_6, δ, ppm): 164.53 (s), 153.83 (s), 135.37 (s), 130.60 (s), 130.24 (s), 128.48 (s), 126.75 (s), 122.25 (s), 115.05 (s).

N2,N6-Bis(4-hydroxyphenyl)pyridine-2,6-dicarboxamide (Compound 6). Compound **6** was synthesized from 2,6-PDCC (5.63 g, 27.6 mmol) according to a method similar to that used for compound **4** (yield: 87%).

Anal. Calcd for $C_{19}H_{15}N_3O_4$: C, 65.32; H, 4.33; O, 18.32; N, 12.03. Found: C, 65.19; H, 4.34; O, 18.40; N, 12.15.

^{1}H NMR (400 MHz, DMSO-d_6, δ, ppm): 10.85 (s, 2H), 9.40 (s, 2H), 8.34 (t, J = 14.1 Hz, 2H), 8.26 (dd, J = 8.4, 7.0 Hz, 1H), 7.64 (d, J = 8.8 Hz, 4H), 6.83 (d, J = 8.8 Hz, 4H).

^{13}C NMR (400 MHz, DMSO-d_6, δ, ppm): 161.45 (s), 154.58 (s), 149.27 (s), 139.99 (s), 129.66 (s), 125.06 (s), 123.51 (s), 115.37 (s).

N2,N5-Bis(3-(furan-2-ylmethyl)-3,4-dihydro-2H-benzoxazine-8-yl)furan-2,5-dicarboxamide (o-AF-fbz). A 3.40 g sample of furfurylamine (35.1 mmol) was dissolved in 250 mL of 1,4-dioxane before it was cooled to 0 °C. Then 5.9 mL of formaldehyde (80.1 mmol) was added dropwisely and the reaction was conducted at 0 °C for one

DOI: 10.1021/acs.macromol.8b00741
Macromolecules XXXX, XXX, XXX−XXX

more hour. After the as-synthesized compound **1** (5.12 g, 15.1 mmol) was added, the reaction temperature was increased up to 105 °C and maintained at this temperature for 20 h. Then the solvent was evaporated under vacuum. The obtained liquid was washed by sodium hydroxide (4% w/w) to eliminate the residual starting materials and dried over anhydrous magnesium sulfate. At last, the precipitate was collected by filtration and dried in the vacuum oven to obtain the light yellow powder (yield: 29%).

Anal. Calcd for $C_{32}H_{28}N_4O_7$: C, 66.20; H, 4.86; O, 19.29; N, 9.65. Found: C, 66.19; H, 4.84; O, 19.40; N, 9.55.

FT-IR (KBr, cm^{-1}): 925, 1340, and 1362.

^1H NMR (400 MHz, $CDCl_3$, δ, ppm): 8.58 (s, 2H), 8.32 (d, J = 7.5 Hz, 2H), 7.40 (t, J = 4.0 Hz, 2H), 7.31 (d, J = 5.2 Hz, 2H), 6.96 (dd, J = 18.4, 10.5 Hz, 2H), 6.77 (d, J = 7.0 Hz, 2H), 6.32 (dt, J = 10.5, 5.3 Hz, 2H), 6.27 (t, J = 8.8 Hz, 2H), 5.01 (s, 4H), 4.03 (s, 4H), 3.92 (s, 4H).

^{13}C NMR (400 MHz, $CDCl_3$, δ, ppm): 155.23 (s), 151.29 (s), 149.03 (s), 142.85 (s), 125.70 (s), 123.06 (s), 120.88 (s), 119.41 (s), 118.78 (s), 116.60 (s), 110.30 (s), 109.23 (s), 83.03 (s), 49.11 (s), 48.53 (s).

N1,N3-Bis(3-(furan-2-ylmethyl)-3,4-dihydro-2H-benzoxazine-8-yl)isophthalamide (o-AB-fbz). *o*-AB-fbz was obtained following a synthesis procedure similar to that used for *o*-AF-fbz, except for the as-synthesized compound 2 (5.29 g, 15.2 mmol) was taken to replace compound 1. After purified and dried in vacuum oven, a yellow powder was obtained (yield: 32%).

Anal. Calcd for $C_{34}H_{30}N_4O_6$: C, 69.14; H, 5.12; O, 16.25; N, 9.49. Found: C, 69.19; H, 5.22; O, 16.21; N, 9.44.

FT-IR (KBr, cm^{-1}): 925, 1340, and 1362.

^1H NMR (400 MHz, $CDCl_3$, δ, ppm): 8.51 (s, 2H), 8.45 (s, 1H), 8.38 (d, J = 8.0 Hz, 2H), 8.10 (dd, J = 7.8, 1.7 Hz, 2H), 7.65 (dd, J = 16.0, 8.2 Hz, 1H), 7.41 (t, J = 7.1 Hz, 2H), 6.96 (t, J = 7.9 Hz, 2H), 6.77 (d, J = 7.3 Hz, 2H), 6.34 (dd, J = 3.1, 1.9 Hz, 2H), 6.26 (d, J = 3.0 Hz, 2H), 5.02 (s, 4H), 4.07 (s, 4H), 3.96 (s, 4H).

^{13}C NMR (400 MHz, $CDCl_3$, δ, ppm): 164.35 (s), 151.30 (s), 142.79 (s), 135.86 (s), 130.24 (s), 129.35 (s), 126.33 (s), 122.66 (s), 120.68 (s), 119.22 (s), 118.42 (s), 110.26 (s), 109.12 (s), 82.88 (s), 49.00 (s), 48.38 (s).

N2,N6-Bis(3-(furan-2-ylmethyl)-3,4-dihydro-2H-benzoxazine-8-yl)pyridine-2,6-dicarboxamide (o-AP-fbz). *o*-AP-fbz was obtained following a synthesis procedure similar to that used for *o*-AF-fbz, except for the as-synthesized compound **3** (5.17 g, 14.8 mmol) that was taken to replace compound **1**. After the reaction product was purified and dried under vacuum, a yellow powder was achieved (yield: 26%).

Anal. Calcd for $C_{33}H_{29}N_5O_6$: C, 67.00; H, 4.94; O, 16.23; N, 11.84. Found: C, 66.70; H, 5.02; O, 16.41; N, 11.76.

FT-IR (KBr, cm^{-1}): 925, 1340, and 1362.

^1H NMR (400 MHz, $CDCl_3$, δ, ppm): 9.97 (s, 2H), 8.49 (d, J = 7.8 Hz, 2H), 8.35 (t, J = 7.5 Hz, 2H), 8.17−8.10 (m, 1H), 7.36−7.30 (m, 2H), 7.02−6.96 (m, 2H), 6.79 (d, J = 7.6 Hz, 2H), 6.28−6.23 (m, 2H), 6.19 (t, J = 6.4 Hz, 2H), 4.95 (s, 4H), 4.01 (s, 4H), 3.90 (s, 4H).

^{13}C NMR (400 MHz, $CDCl_3$, δ, ppm): 161.49 (s), 151.27 (s), 149.63 (s), 143.82 (s), 142.76 (s), 139.48 (s), 125.90 (s), 125.59 (s), 123.22 (s), 120.81 (s), 119.53 (s), 110.35 (s), 109.23 (s), 83.08 (s), 49.21 (s), 48.44 (s).

N2,N5-Bis(3-(furan-2-ylmethyl)-3,4-dihydro-2H-benzoxazine-6-yl)furan-2,5-dicarboxamide (p-AF-fbz). *p*-AF-fbz was synthesized from compound **4** (5.02 g, 14.9 mmol) following a synthesis procedure similar to that used for *o*-AF-fbz (yield: 21%).

Anal. Calcd for $C_{32}H_{28}N_4O_7$: C, 66.20; H, 4.86; O, 19.29; N, 9.65. Found: C, 66.15; H, 4.91; O, 19.36; N, 9.59.

FT-IR (KBr, cm^{-1}): 928, 1340, and 1363.

^1H NMR (400 MHz, $CDCl_3$, δ, ppm): 8.80 (s, 2H), 7.44 (s, 2H), 7.41 (d, J = 1.0 Hz, 2H), 7.23 (s, 2H), 6.75 (d, J = 8.7 Hz, 2H), 6.35−6.32 (m, 2H), 6.25 (d, J = 3.0 Hz, 2H), 4.84 (s, 4H), 3.98 (s, 4H), 3.89 (s, 4H).

^{13}C NMR (400 MHz, $CDCl_3$, δ, ppm): 156.15 (s), 151.86 (s), 151.64 (s), 149.05 (s), 143.06 (s), 130.62 (s), 121.27 (s), 120.79 (s), 120.47 (s), 117.21 (s), 116.57 (s), 110.71 (s), 109.53 (s), 82.30 (s), 49.97 (s), 48.66 (s).

N1,N3-Bis(3-(furan-2-ylmethyl)-3,4-dihydro-2H-benzoxazine-6-yl)isophthalamide (p-AB-fbz). *p*-AB-fbz was synthesized from compound 5 (5.16 g, 14.8 mmol) following following a synthesis procedure similar to that used for *p*-AF-fbz (yield: 16%).

Anal. Calcd for $C_{34}H_{30}N_4O_6$: C, 69.14; H, 5.12; O, 16.25; N, 9.49. Found: C, 69.22; H, 5.14; O, 16.35; N, 9.31.

FT-IR (KBr, cm^{-1}): 928, 1340, and 1363.

^1H NMR (400 MHz, $CDCl_3$, δ, ppm): 8.34 (s, 1H), 8.15 (s, 2H), 8.00 (d, J = 7.6 Hz, 2H), 7.56 (t, J = 7.7 Hz, 1H), 7.42 (s, 4H), 7.24 (s, 2H), 6.79 (d, J = 8.7 Hz, 2H), 6.39−6.33 (m, 2H), 6.27 (d, J = 3.0 Hz, 2H), 4.87 (s, 4H), 4.00 (s, 4H), 3.91 (s, 4H).

^{13}C NMR (400 MHz, $CDCl_3$, δ, ppm): 165.29 (s), 151.90 (s), 151.62 (s), 143.11 (s), 135.81 (s), 131.19 (s), 130.77 (s), 129.76 (s), 125.91 (s), 121.16 (s), 120.60 (s), 117.33 (s), 110.71 (s), 109.55 (s), 82.35 (s), 50.11 (s), 48.68 (s).

N2,N6-bis(3-(furan-2-ylmethyl)-3,4-dihydro-2H-benzoxazine-6-yl)pyridine-2,6-dicarboxamide (p-AP-fbz). *p*-AP-fbz was synthesized from compound 6 (5.24 g, 15.0 mmol) following following a synthesis procedure similar to that used for *p*-AF-fbz (yield: 17%).

Anal. Calcd for $C_{33}H_{29}N_5O_6$: C, 67.00; H, 4.94; O, 16.23; N, 11.84. Found: C, 66.85; H, 5.09; O, 16.46; N, 11.73.

FT-IR (KBr, cm^{-1}): 928, 1340, and 1363.

^1H NMR (400 MHz, $CDCl_3$, δ, ppm): 9.45 (s, 2H), 8.44 (t, J = 9.2 Hz, 2H), 8.10 (t, J = 7.8 Hz, 1H), 7.54 (d, J = 2.3 Hz, 2H), 7.42 (d, J = 1.1 Hz, 2H), 7.33 (dd, J = 8.7, 2.4 Hz, 2H), 6.81 (t, J = 8.5 Hz, 2H), 6.33 (dd, J = 10.3, 8.4 Hz, 2H), 6.26 (d, J = 3.0 Hz, 2H), 4.88 (s, 4H), 4.02 (s, 4H), 3.92 (s, 4H).

^{13}C NMR (400 MHz, $CDCl_3$, δ, ppm): 161.23 (s), 151.59 (s), 151.42 (s), 149.23 (s), 142.77 (s), 139.64 (s), 130.32 (s), 125.57 (s), 120.70 (s), 120.24 (s), 117.06 (s), 110.39 (s), 109.19 (s), 82.10 (s), 49.79 (s), 48.41 (s).

Curing Procedure. Benzoxazine monomers were melted and transferred to a stainless steel mold as quickly as possible. Then the sample was cured by the programmed temperature rising method: 2 h at 180 °C, 2 h at 200 °C, and 4 h at 220 °C. After curing reaction, the samples were cooled down to the room temperature slowly to prevent cracking. In this work, all of the samples including *o*-AF-fbz, *o*-AB-fbz, *o*-AP-fbz, *p*-AF-fbz, *p*-AB-fbz, and *p*-AP-fbz were cured under the same condition.

Measurements. NMR spectra were recorded on a 400 MHz Bruker AVANCE III spectrometer. It was conducted at 25 °C using DMSO-d_6 or $CDCl_3$ as the solvent. The tetramethysilane (TMS) was used as internal standard and the times of scans was 16. For the 2D $^1H-^1H$ NOESY NMR measurement, related parameters were set as 2048 data points along the $f2$ dimension, 256 free induction decays in the $f1$ dimension, and relaxation delay of 2 s, and the mixing time was 700 ms.

Mass spectra were measured with a LC-Q-TOF (AB Sciex, America) using ionization at 500 °C with an ionization voltage of 5500 V. Elementary analysis (EA) was measured by Elementar (Elementar, Germany).

Fourier transform infrared (FT-IR) spectra were recorded in transmission mode using a Thermo Nicolet 6700 Fourier transform infrared spectrometer (Thermo-Fisher Scientific). Samples were powdered and dispersed into a KBr matrix with a weight concentration of about 1 wt %. Spectra were scanned from 400 to 4000 cm^{-1} with 32 scans collected for each sample. For the in situ FT-IR measurement at various temperature (50, 100, 150, 200, and 250 °C). Cured samples were inserted into a hot cell which was adapted to the FT-IR spectrometer, and the scan was started as soon as the hot cell temperature reached the desired temperature.

The DSC measurement was conducted on a METTLER TOLEDO-TGA/DSC I under a nitrogen atmosphere flow rate of 20 mL min^{-1}. Approximately 5−10 mg of each sample was weighed and sealed in 40 μL aluminum crucibles. The sample was heated from 50 to 300 °C at the heating rate of 10 °C min^{-1}. In order to determine the activation energy of polymerization, the DSC measurement was conducted at different heating rates of 2,5, 10, and 20 °C min^{-1}. DSC

DOI: 10.1021/acs.macromol.8b00741
Macromolecules XXXX, XXX, XXX−XXX

Scheme 2. Synthetic Route for the Model Benzoxazine Monomers Containing Amide Groups at *ortho*- and *para*-Positions with Respect to the Oxygen Atom (*o*-AF-fbz, *o*-AB-fbz, *o*-AP-fbz, *p*-AF-fbz, *p*-AB-fbz, and *p*-AP-fbz)

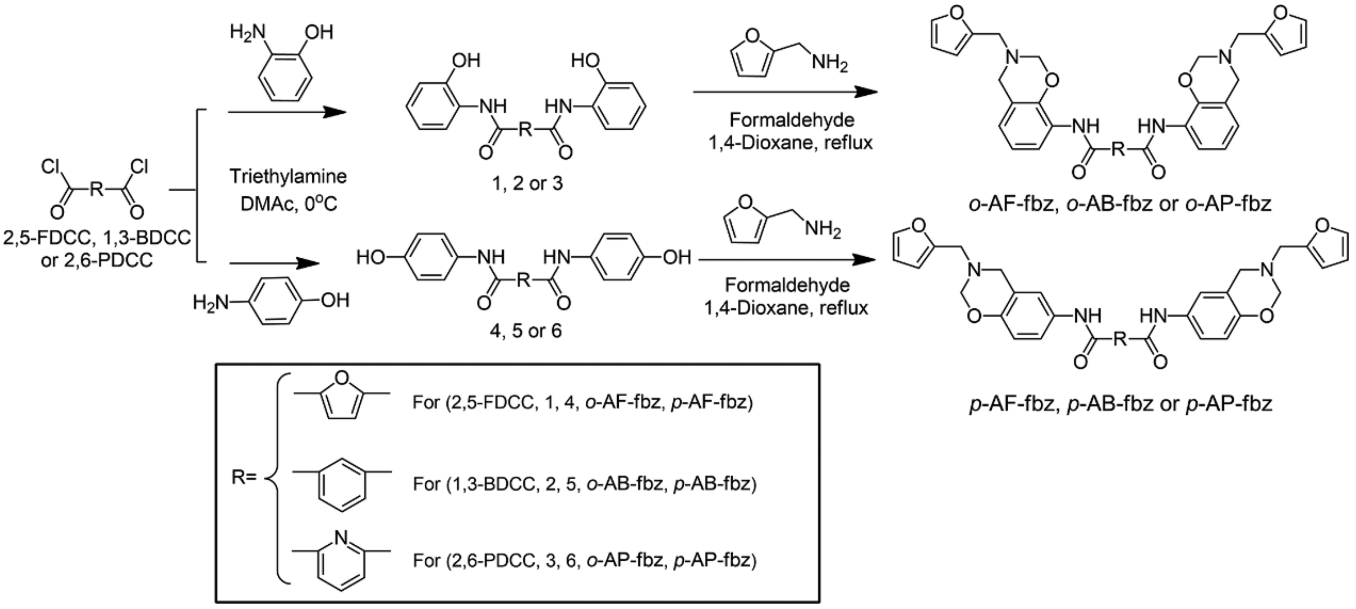

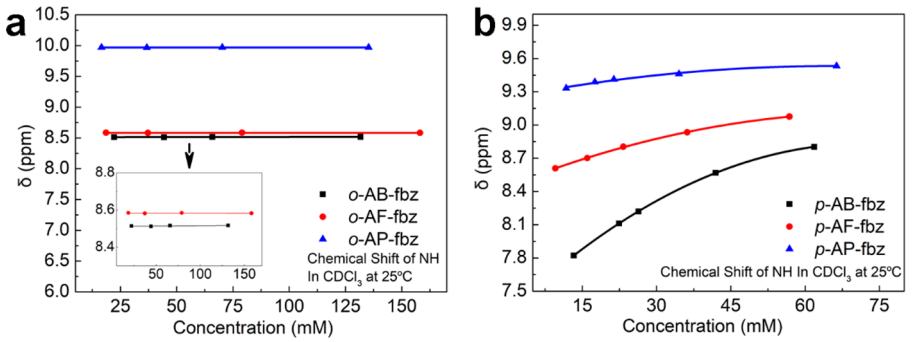

Figure 1. Variation of the chemical shift of NH in *o*-AB-fbz (a), *o*-AF-fbz (a), *o*-AP-fbz (a), *p*-AB-fbz (b), *p*-AF-fbz (b), and *p*-AP-fbz (b) as a function of concentration in $CDCl_3$ at 25 °C.

analysis was repeated twice for each sample to ensure the accuracy. TGA measurement was conducted on a Mettler-Toledo TGA/DSC1 thermogravimetric analyzer (METTLER TOLEDO, Switzerland) with high purity nitrogen or air as purge gas (50 mL min^{-1}) at a scanning rate of 20 °C min^{-1} from 50 to 800 °C. DMA was performed on Mettler-Toledo DMAQ800 under a tensile mode at a frequency of 1 Hz with the amplitude of 5 μm. The test samples were scanned from 0 to 360 °C at a heating rate of 3 °C min^{-1}. Each sample was tested three times to ensure the accuracy.

Simulation. The MD simulations are carried out with the Materials Studio 7.0 (Accelrys. Inc.).[53] The partial charges on the molecules are obtained from iterative partial equalization of orbital electronegativity via Gasteiger method.[54] The nonbonded interactions are calculated from the Lennard-Jones (12−6) potential function and group-based summation for van der Waals and electrostatic interactions, respectively, with the cutoff set at 1.2 nm for both types of interactions. The temperature of simulation box is controlled using Nosé−Hoover−Langevin (NHL) thermostat with a *Q* ratio of 0.01.[55] For the pressure control in *NPT*-MD simulations (constant pressure, temperature and number of particles), the Parrinello−Rahman barostat was taken.[56−58] All the model systems in this study consist of 100 monomer molecules per simulation box for each studied resin. The size of the simulation box is ∼5 nm. The cross-link networks are constructed using the cyclic polymerization atomistic model with conducted multistep topology relaxation. The detailed procedures are following the previous work.[48]

RESULTS AND DISCUSSION

Synthesis and Characterization of Model Benzoxazine Monomers. Scheme 2 illustrated the synthesis of *o*-AF-fbz, *o*-AB-fbz, *o*-AP-fbz, *p*-AF-fbz, *p*-AB-fbz, and *p*-AP-fbz. Started from different dicarboxylic acids (IPA, 2,5-FDCA and 2,6-PDCA), six kinds of bisphenol monomers containing amide group were synthesized. Then, they were reacted with formaldehyde in the solution of 1,4-dioxane and the target products were obtained. The detailed synthesis procedures were described in the Experimental Section, and the Supporting Information, Figure S1−S12, showed the ^1H and ^{13}C NMR spectra of all the synthesized compounds. Besides this , the mass spectrometry of the six model benzoxazine monomers, *o*-AF-fbz, *o*-AB-fbz, *o*-AP-fbz, *p*-AF-fbz, *p*-AB-fbz, and *p*-AP-fbz were also collected in Supporting Information (Figure S13−S18)). These chemical structure confirmation indicated the high purity of final products and ensured the investigation on the relationship between their chemical structures and curing behaviors.

On the basis of the chemical structure analysis of *o*-AF-fbz, *o*-AB-fbz, *o*-AP-fbz, *p*-AF-fbz, *p*-AB-fbz, and *p*-AP-fbz, it was easy to speculate the presence of inter- or intramolecular H-bonding in them, easily formed between the electron acceptor

DOI: 10.1021/acs.macromol.8b00741
Macromolecules XXXX, XXX, XXX−XXX

Scheme 3. Proposed H-Bonding Interactions in *o*-AB-fbz, *o*-AF-fbz, *o*-AP-fbz, *p*-AB-fbz, *p*-AF-fbz, and *p*-AP-fbz[a]

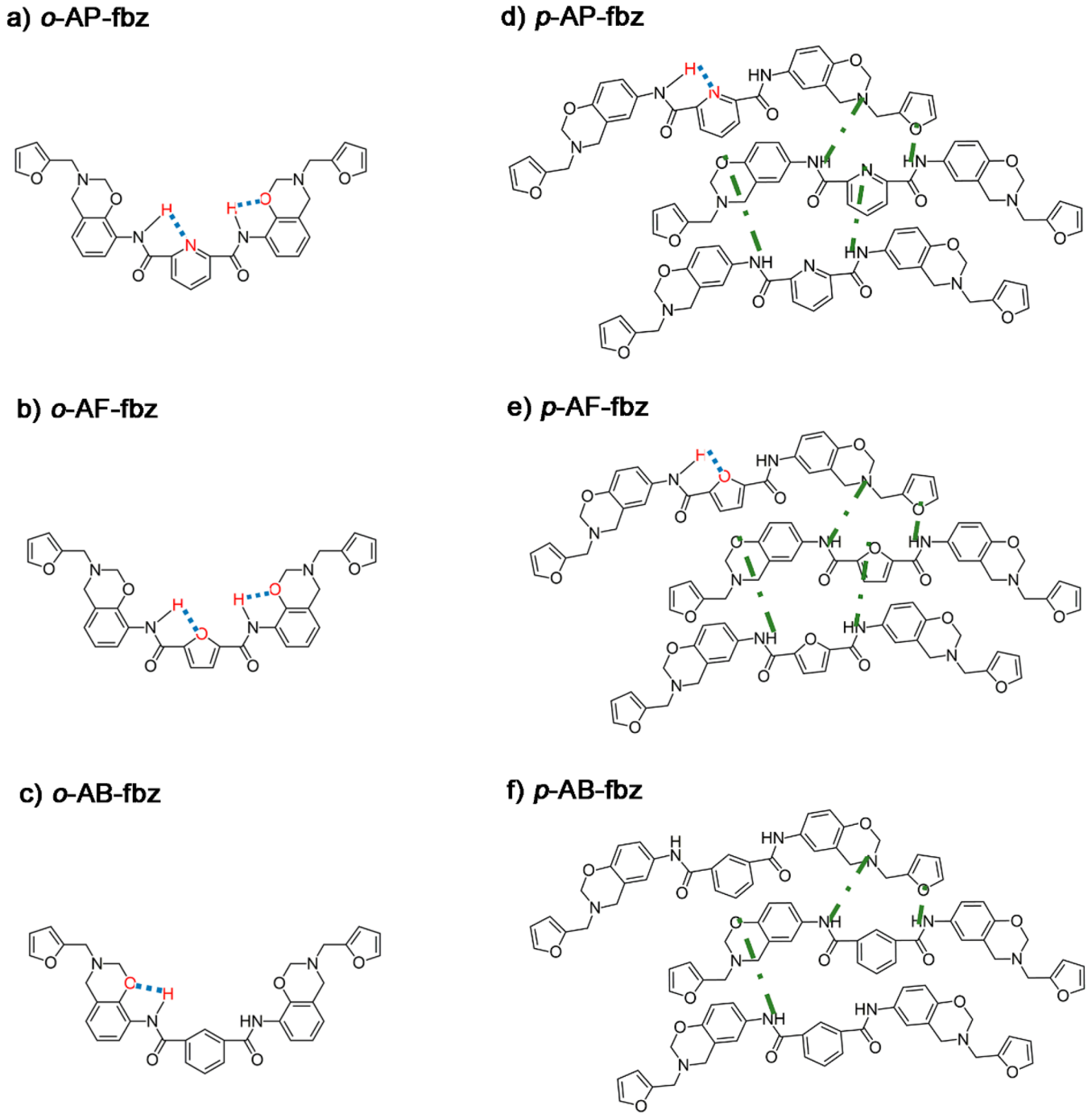

[a]Green square-dotted intervening with round-dotted lines depict intermolecular H-bonding, while blue round-dotted lines represent the intramolecular H-bonding. (For easy identification, the H-bondings related to the furfurylamine structure as well as other possible H-bondings were not illustrated, due to their low strength.)

of −CON*H*− and electron donors of *O* in furan ring and *N* in pyridine ring. As we know, for the ^{1}H NMR spectrum, the used solvent and concentration as well as temperature will strongly influence the signal quality and chemical shift of N*H*. Also, the formation of H-bonding is another factor to determine its chemical shift. For example, in the case of intermolecular H-bonding, the chemical shift of N*H* will move to a higher ppm with the increased concentration because of the decreased average of hydrogen-bonding distance. While the intramolecular hydrogen-bonded systems will not be affected by the concentration. Therefore, through the ^{1}H NMR experiments, the inter- and intramolecular H-bonding in the solution could be analyzed.[27,29,30,41] For instance, Ishida and his coworkers[29] once characterized the chemical shifts of O*H* in methylol groups at the *ortho*- or *para*-position with respect to the oxazine ring as a function of concentration in $CDCl_3$ at 25 °C. On the basis of which, they confirmed that the signals for intramolecular hydrogen bonded OH showed nearly no change upon the increment of concentration. While the O*H* signals related to the intermolecular H-bonding demonstrated a

DOI: 10.1021/acs.macromol.8b00741
Macromolecules XXXX, XXX, XXX−XXX

significant chemical shift toward downfield when the concentration was increased. In this work, the variation of the chemical shift of N*H* at different solution concentration was also studied. Figure 1a showed the chemical shifts of N*H* in *o*-AB-fbz, *o*-AF-fbz, and *o*-AP-fbz as a function of concentration, obtained from ^{1}H NMR spectra using $CDCl_3$ as the solvent at 25 °C. The independence of the N*H* chemical shift in *o*-AB-fbz, *o*-AF-fbz, and *o*-AP-fbz with respect to concentration clearly indicated that no intermolecular H-bonding were formed within the studied concentration range. Moreover, the high chemical shifts of these particular N*H* groups (8.51 ppm for *o*-AB-fbz, 8.58 ppm for *o*-AF-fbz and 9.97 ppm for *o*-AP-fbz) suggested that the protons were, in fact, participating in the intramolecular H-bonding.[27,30] And it might be due to the higher negative electron density of N atom in o-AP-fbz, the proton in amide group (−CON*H*−) was more strongly deshielded and its chemical shift was high up to 9.97 ppm, which might indicate the stronger H-bonding. In the case of *o*-AB-fbz and *o*-AF-fbz, the interaction between the proton (−CON*H*−) and O atoms (no matter it is in the furan ring or oxazine ring) might be same. Therefore, nearly no difference in the chemical shift of N*H* was observed. Different from Figure 1a, Figure 1b indicated that the chemical shift of the N*H* group in *p*-AB-fbz, *p*-AF-fbz, and *p*-AP-fbz was influenced in different degree by the solution concentration. In particualr, in *p*-AB-fbz, the ^{1}H NMR signal for N*H* was shifted from 7.8 to 8.7 ppm when the concentration was increased from 15 to 65 Mm. And in the system of *p*-AF-fbz and *p*-AP-fbz, the signals for N*H* showed a relatively weak dependence on the concentration, indicated by the smaller slopes of red and blue lines in Figure 1b. In Ishida's work,[29] they also reported the similar results that the signal for O*H* in *ortho*-positioned methylol groups was independent of the concentration at first and when the concentration was higher than 2.5 mM, the weak dependence was noticed. And this result was attributed to the competition between inter- and intramolecular H-bonding. That was to say the inter- and intramolecular hydrogen bonding existed simultaneously. In our work, the dependence of N*H* chemical shift for *p*-AB-fbz, *p*-AF-fbz, and *p*-AP-fbz upon concentration was undoubtedly an indication for the intermolecular H-bonding. Besides that, the varying degrees of concentration dependence for N*H* chemical shift indicated the simultaneous existence of inter- and intramolecular H-bonding as well as the different ratio of them in *p*-AB-fbz, *p*-AF-fbz, and *p*-AP-fbz. The fraction of intermolecular H-bonding should follow the order of *p*-AB-fbz > *p*-AF-fbz > *p*-AP-fbz, based on the degree of concentration dependence showing in Figure 1b.

Scheme 3 depicted the proposed inter- and intramolecular H-bonding interactions mainly involved with the various central moieties (benzene, furan and pyridine moieties) and amide group in *o*-AB-fbz, *o*-AF-fbz, *o*-AP-fbz, *p*-AB-fbz, *p*-AF-fbz and *p*-AP-fbz. For easy identification, the H-bonding related to furfurylamine structure as well as other possible H-bonding were not illustrated, due to their low strength. In the case of *o*-AB-fbz, *o*-AF-fbz, and *o*-AP-fbz, the N*H* groups tended to participate in intramolecular H-bonding with the oxygen atom in oxazine ring, oxygen in furan or nitrogen in pyridine ring. And due to the formation of strong and stable five-membered ring, the intermolecular H-bonding interactions were difficult to take place. That was to say the intramolecular H-bonding was dominant in *o*-AB-fbz, *o*-AF-fbz and *o*-AP-fbz, which was consistent with the results from Figure 1a. As for *p*-AP-fbz and *p*-AF-fbz, the five-membered intramolecular H-bonding could be formed between the N*H* groups and nitrogen in pyridine as well as oxygen atom in the furan ring. At higher concentrations, the intermolecular H-bonding would form when the intermolecular distance became short enough. Therefore, the intermolecular and intramolecular hydrogen bondings existed simultaneously. However, in the system of *p*-AB-fbz, only intermolecular hydrogen bonding could be formed.

Although above results confirmed that N*H* groups in *o*-AB-fbz, *o*-AF-fbz and *o*-AP-fbz participated in intramolecular H-bonding, there was no indication about the possibility of breaking or disrupting the H-bonding interactions. In other words, no information had yet been obtained to clarify whether all of the N*H* protons participated in the formation of H-bonding or not. This fact was related to the strength or stability of the intramolecular H-bonding in *o*-AB-fbz, *o*-AF-fbz, and *o*-AP-fbz. To address this question, ^{1}H−^{1}H nuclear overhauled effect spectroscopy (NOESY), a 2D NMR technique which can provide structural information by through-space interactions,[27,59,60] was carried out and the results were presented in Figure 2.

In *o*-AB-fbz, besides the H-bonding, the protons in amide group (−CON*H*) also have interactions with the proton at position-1 (H_1) in oxazine ring, aromatic protons at position-2 (H_2) and position-3 (H_3), which was supported by the signals in Figure 2a (marked as dots 1, 2, 3 in red type, respectively). Similar interactions were also observed for *o*-AF-fbz (Figure 2b) and *o*-AP-fbz (Figure 2c). This result indicated the presence of free N*H* protons, which did not participate in the H-bonding formation. As we know, the signal intensity reflects the strength or intensity of through-space interaction. The higher signal intensity, the stronger or more interaction.[48] When the intensities of signal 1 and signal 2 in parts a−c ofFigure 2 were compared, from *o*-AB-fbz to *o*-AP-fbz, the through-space interaction followed the order of *o*-AB-fbz > *o*-AF-fbz > *o*-AP-fbz and demonstrated that the strength of overall intramolecular H-bonding was in the order of *o*-AB-fbz < *o*-AF-fbz < *o*-AP-fbz. This result was reasonable based on their chemical structures analysis. In *o*-AF-fbz and *o*-AP-fbz, besides the oxygen atom in oxazine ring, the oxygen atom in furan ring and nitrogen atom in pyridine ring would also tend to participate in the five-membered H-bonding formation with N*H* group. The N*H* proton attraction competition between these different electron-donors was inevitable and due to the higher basicity of pyridine ring, the RCON−H--N (pyridine) interaction might be stronger than RCON−H--O (furan). Therefore, the strength of intramolecular hydrogen bonding between N*H* group and oxygen in oxazine ring would be different, which would dramatically influence the curing behaviors of benzoxazines.[27,29,30] And in the following section, the curing behaviors of synthesized model benzoxazine precursors will be investigated. For easy identification, the possible different intra- and intermolecular H-bonding as well as their strength comparison in *o*-AB-fbz, *o*-AF-fbz, *o*-AP-fbz, *p*-AB-fbz, *p*-AF-fbz, and *p*-AP-fbz were briefly illustrated in Figure 3. From red to violet, the strength of different type H-bonding was qualitatively represented by the different colors.

Curing Behaviors of Model Benzoxazines. The curing behaviors of *o*-AB-fbz, *o*-AF-fbz, *o*-AP-fbz, *p*-AB-fbz, *p*-AF-fbz, and *p*-AP-fbz were investigated by DSC. As marked in Figure 4, the peak exothermic temperatures for *o*-AB-fbz, *o*-AF-fbz, *o*-AP-fbz, *p*-AB-fbz, *p*-AF-fbz, and *p*-AP-fbz were 211, 218, 227, 233, 238, and 241 °C, respectively. And the onset curing

DOI: 10.1021/acs.macromol.8b00741
Macromolecules XXXX, XXX, XXX−XXX

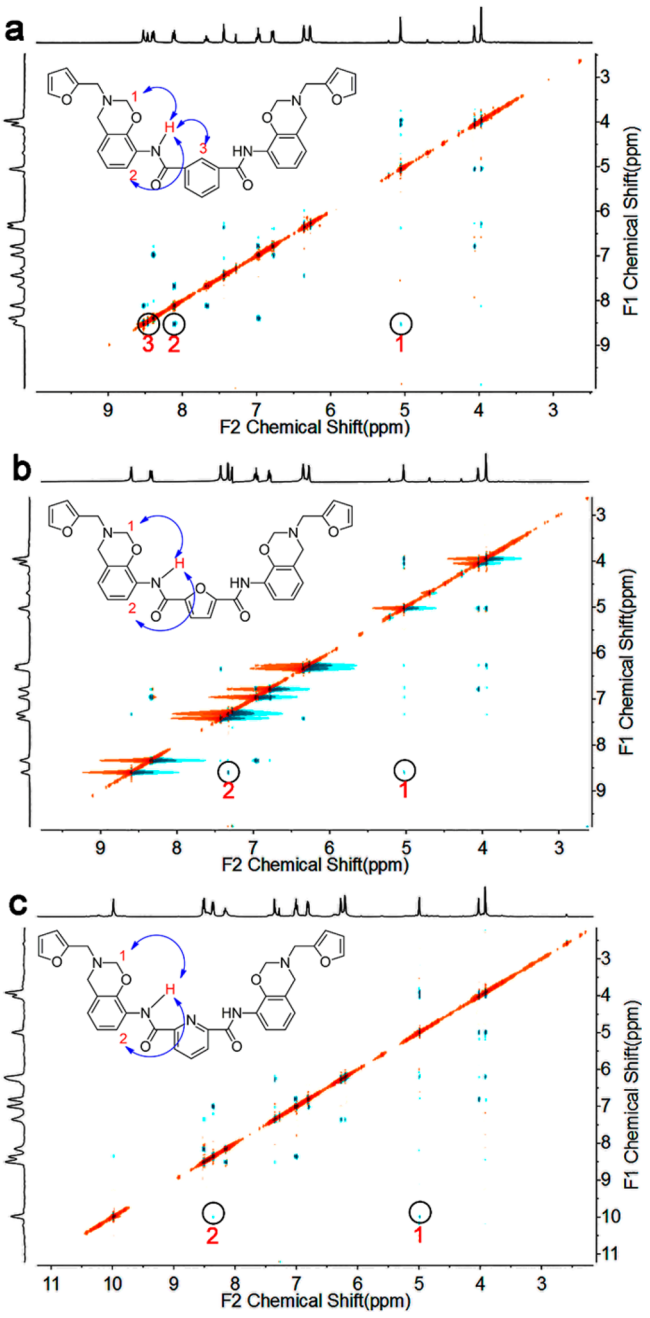

Figure 2. 2D $^{1}H-^{1}H$ NOESY NMR spectra of *o*-AB-fbz (a), *o*-AF-fbz (b), and *o*-AP-fbz (c) in $CDCl_3$.

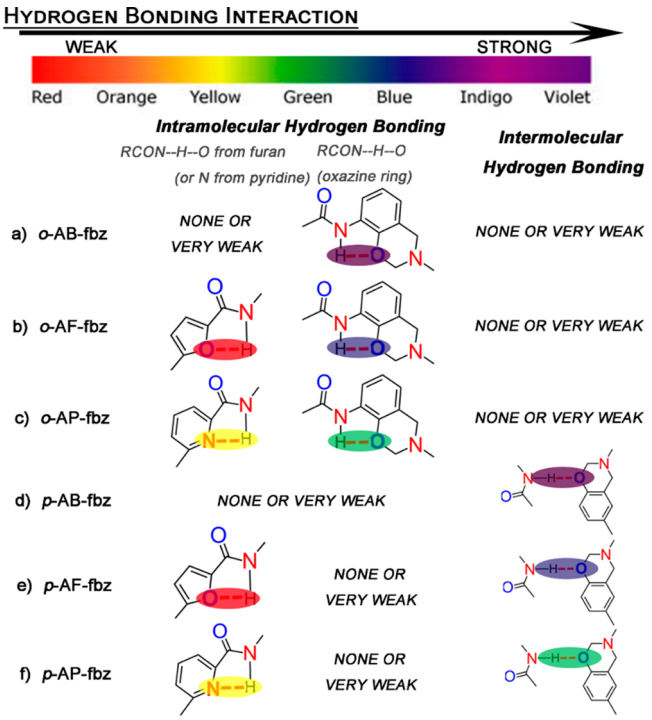

Figure 3. Illustration of different intra- and intermolecular hydrogen bonding and the qualitative strength comparison between them in *o*-AB-fbz, *o*-AF-fbz, *o*-AP-fbz, *p*-AB-fbz, *p*-AF-fbz, and *p*-AP-fbz. (RCON−H--O from oxazine ring as an example for intermolecular hydrogen bonding).

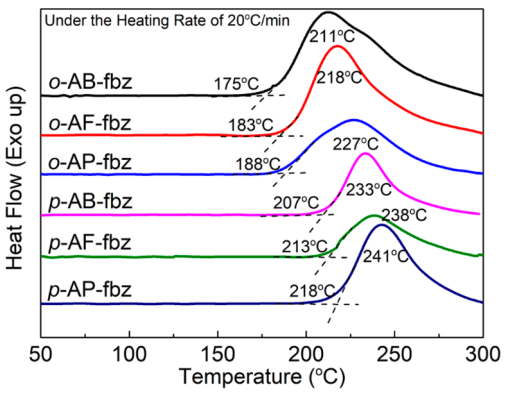

Figure 4. DSC heating curves of different precursors.

temperatures of them followed the same order (175 °C for *o*-AB-fbz, 183 °C for *o*-AF-fbz, 188 °C for *o*-AP-fbz, 207 °C for *p*-AB-fbz, 213 °C for *p*-AF-fbz and 218 °C for *p*-AP-fbz). What should be mentioned was that the melting endotherms, usually taken as a parameter for monomer purity evaluation, were absent in the DSC scan. It is well-known that, the impurities will influence the performance of cured benzoxazine resins seriously, including the curing property. Besides the NMR, FT-IR, elementary analysis and mass spectra (Supporting Information, Figures S13−S18) measurements, in order to further confirm the purity of the synthesized monomers, *o*-AB-fbz and *p*-AB-fbz were applied for several purification treatments and after each purification, the DSC measurement was conducted and the curves were collected for comparison (Supporting Information, Figure S19). Although all the DSC thermograms did not show any melting endotherms, possibly attributed to the influence of amide groups,[55] the heating curves of *o*-AB-fbz and *p*-AB-fbz after several times purification showed similar peak exothermic temperatures, which confirmed the high purity of the synthesized monomers again. As we know, under the same curing condition, the onset and peak curing temperature can be taken as an indicator for curing reactivity evaluation. The higher the onset or peak curing temperature, the lower curing reactivity.[61] Apparently, the *ortho*-positioned systems (*o*-AB-fbz, *o*-AF-fbz, and *o*-AP-fbz) showed higher curing reactivity when compared with those of the *para*-substituted systems (*p*-AB-fbz, *p*-AF-fbz, and *p*-AP-fbz). In addition, for the *ortho*-substituted systems, their curing activities followed the order of *o*-AB-fbz > *o*-AF-fbz > *o*-AP-fbz. And the *para*-substituted systems were arranged as follows: *p*-AB-fbz > *p*-AF-fbz > *p*-AP-fbz. It was noted that the curing

DOI: 10.1021/acs.macromol.8b00741
Macromolecules XXXX, XXX, XXX−XXX

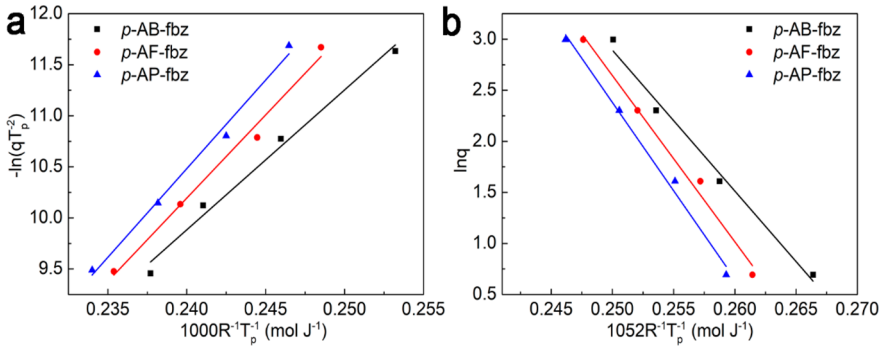

Figure 5. Plots of $-\ln(qT_p^{-2})$ versus 1000 $R^{-1}T_p^{-1}$ (a) and ln q versus 1052 $R^{-1}T_p^{-1}$ (b).

activities followed the same order of H-bonding strength involved with the oxygen atoms in oxazine ring, rather than the strength of overall H-bonding, in the model benzoxazines.[62]

In order to further confirm the curing reactivity comparison, the Kissinger and Ozawa methods, which are considered to be the simple approaches to quantify a complex thermoset curing process, were employed.[63−65] For research convenience, only the *para*-substituted systems (*p*-AB-fbz, *p*-AF-fbz and *p*-AP-fbz) were applied for the Kissinger and Ozawa method investigation. The Kissinger method[63] is based on a linear relationship between logarithm of (qT_p^{-2}) and T_p^{-1} and can be explained by the following eq 1:

$$\ln\left(\frac{q}{T_p^2}\right) = \ln\left(\frac{AR}{E_a}\right) - \frac{E_a}{RT_p} \quad (1)$$

where T_p was the peak exothermic temperature (K), q was the heating rate (°C min^{-1}), E_a was an average activation energy of the curing reaction (J mol^{-1}), A was the pre-exponential factor (min^{-1}), and R was the universal gas constant with a value of 8.314 J mol^{-1} K^{-1}. T_p and its corresponding heating rate (q) could be obtained from Figure S20 (Supporting Information) and the activation energy could be calculated from the slope of the plots of $-\ln(qT_p^{-2})$ versus T_p^{-1} (Figure 5a).

The modified Ozawa method[64] is another way to determine the E_a, based on eq 2:

$$\ln q = \ln\left(\frac{AE_a}{R}\right) - \ln g(\alpha) - 5.331 - 1.052\left(\frac{E_a}{RT_p}\right) \quad (2)$$

where $g(\alpha) = \int_0^\alpha \frac{d\alpha}{f(\alpha)} = -\ln(1-\alpha)$ was the integral conversion function. E_a could be derived from the slope of ln q against T_p^{-1} plots (Figure 5b). The different heating rates (q) and corresponding T_p as well as E_a obtained via Kissinger and modified Ozawa methods were summarized in Table 1. It was noticed that the activation energy of *p*-AB-fbz was the lowest, indicating the highest curing reactivity. While *p*-AP-fbz showed the lowest curing activity indicating by the highest activation energy. This was in a good agreement with the result obtained from Figure 4 and the above curing reactivity comparison was proved to be reliable. It was noted that all the samples showed an activation energy a little higher than the typical value for benzoxazine polycondensation (130−90 kJ/mol). The reason might be that, besides the oxazine ring-opening reaction, the furfural group participated in the side reaction, which led to a higher observed activation energy.

In Ishida's work,[30] the higher curing reactivity of *ortho*-amide functional benzoxazine was attributed to the acceleration effect of intramolecular five-membered H-bonding formed between the N*H* in amide group and the oxygen in oxazine ring. In this work, the intra- and intermolecular H-bonding in the model benzoxazines was clearly identified and the higher curing reactivity of *ortho*-substituted systems was undoubtedly related to the H-bonding. As illustrated in Figure 3, in the *o*-amide systems (*o*-AB-fbz, *o*-AF-fbz, and *o*-AP-fbz), not only the oxygen in the oxazine ring participated in the intramolecular hydrogen bonding, but also the nitrogen atom in pyridine and oxygen in furan ring did. And due to the higher proton withdrawing ability of pyridine, the RCON−H--N (pyridine) interaction was stronger than that of RCON−H--O (furan) and RCON−H--O (Ar). Therefore, the strength of the five-membered intramolecular H-bonding formed between RCON*H* and the oxygen in oxazine ring should follow the order of *o*-AB-fbz > *o*-AF-fbz > *o*-AP-fbz. On the basis of the proposed curing mechanism in literatures,[23,27,29−31] the catalytic effect of H-bonding in the different systems should follow the same order and the sequence of *o*-AB-fbz > *o*-AF-fbz > *o*-AP-fbz for their curing activities was reasonable. In Scheme 4, the proposed mechanism was illustrated briefly. In the case of *p*-amide systems (*p*-AB-fbz, *p*-AF-fbz, *p*-AP-fbz), due to the presence of furan and pyridine in *p*-AF-fbz and *p*-AP-fbz, respectively. The intramolecular H-bonding (RCON−H--N (pyridine) and RCON−H--O (furan)) could be formed, which would attract and limit the movement of partial protons in RCON-H group, leading to the decreased possibility of intermolecular H-bonding between the oxygen in oxazine

Table 1. E_a Comparison for *para*-Substituted Benzoxazine Determined by Kissinger and the Modified Ozawa Equation

			E_a (kJ mol^{-1})		ln A^a	
samples	heating rates (q) (°C min^{-1})	T_p (K)	Kissinger	Ozawa	Kissinger	Ozawa
p-AB-fbz	2	475	137.0	138.0	32.72	32.64
	5	489				
	10	499				
	20	506				
p-AF-fbz	2	484	162.1	162.2	38.80	38.42
	5	492				
	10	502				
	20	511				
p-AP-fbz	2	488	173.6	173.9	41.13	40.63
	5	496				
	10	505				
	20	514				

[a]The dimension of A is min^{-1}, and α was 0.5.

DOI: 10.1021/acs.macromol.8b00741
Macromolecules XXXX, XXX, XXX−XXX

Scheme 4. Illustration for How the Intramolecular Hydrogen Bonding and Its Strength Influence the Curing of Benzoxazine Precursors (*o*-AB-fbz, *o*-AF-fbz, and *o*-AP-fbz Set as an Example)

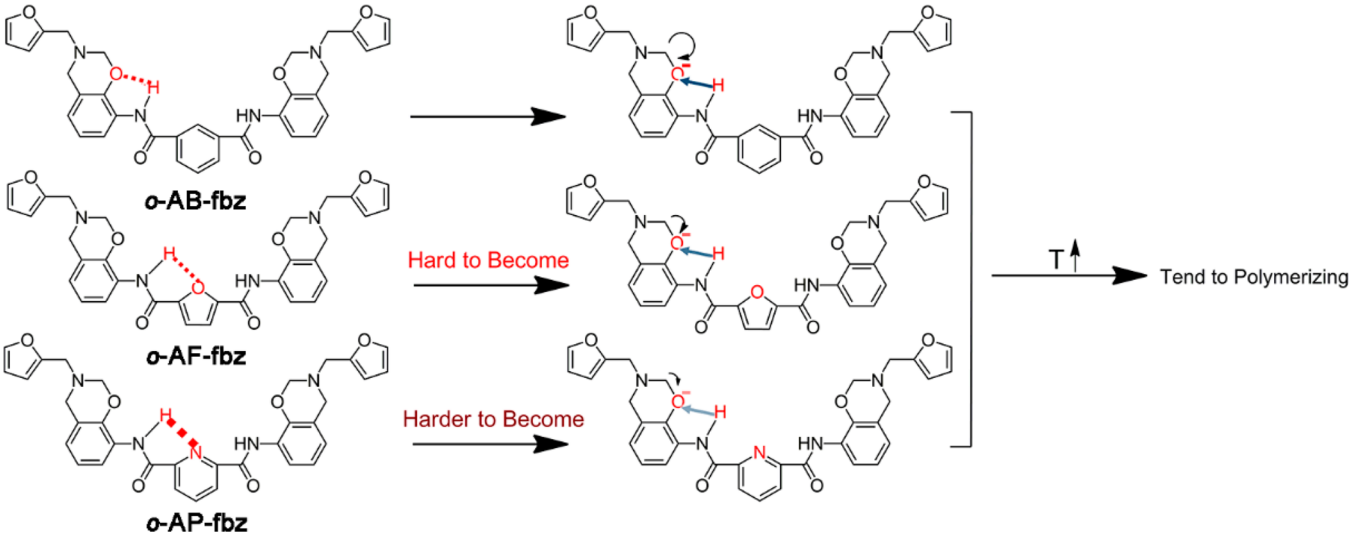

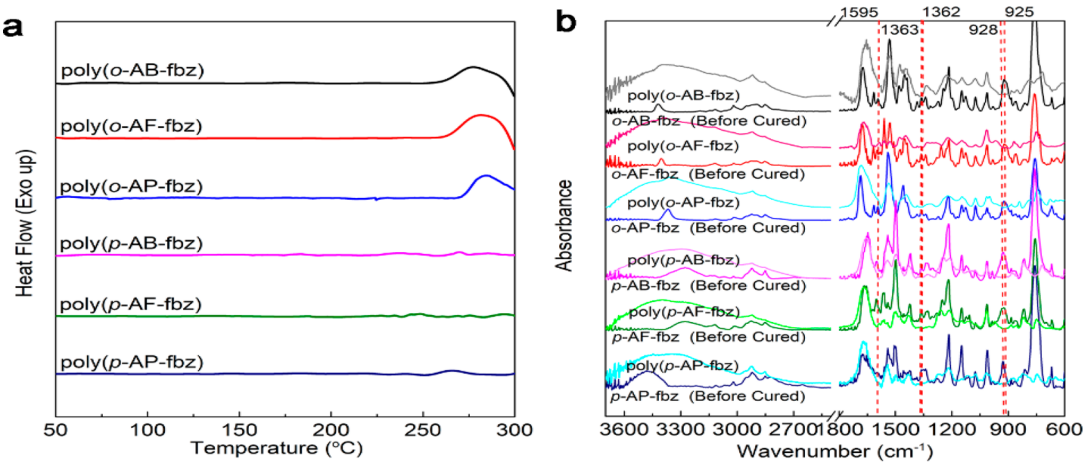

Figure 6. DSC heating curves for the cured benzoxazine networks (a). FT-IR spectra of all the cured benzoxazine networks before and after curing reaction (b).

rings, and then reduced the catalytic effects. However, for the *p*-AB-fbz, all of the protons in NH groups had the opportunity to participate in the formation of intermolecular H-bonding. The strength of intermolecular H-bonding involved with the oxygen in oxazine rings followed the order of *p*-AB-fbz > *p*-AF-fbz > *p*-AP-fbz (Figure 3), which was the reason for the lowest curing temperature of *p*-AB-fbz compared with *p*-AF-fbz and *p*-AP-fbz.

As for the determination of curing condition for benzoxazine precursors, the curing process should be started at a temperature at which the curing reaction is relatively mild. And the temperature for postcuring must be high enough to ensure the full curing reaction in a proper curing time. Additionally, the possible rearrangement under high temperature should be controlled during the curing process. According to previous publication,[55] *ortho*-amide functional polybenzoxazines might suffer rearrangement at around 250 °C to form polybenzoxazole after the polybenzoxazines cured completely. In this work, *o*-AB-fbz, *o*-AF-fbz, and *o*-AP-fbz also possessed *o*-amide groups and the post rearrangement would be inevitable at higher temperature, which was already indicated by the broad peak around 250 °C in the DSC curve for *o*-AB-fbz (Figure 4). The formation of polybenzoxazole structure is not conducive to H-bonding investigation. Therefore, the curing procedures for all the samples were determined as follows: 2 h at 180 °C, 2 h at 200 °C, and 4 h at 220 °C according to the literature.[55] Figure 6a shows the DSC heating curves for all the systems after curing reaction. Before 250 °C, no obvious peaks were observed, which indicated the complete curing reaction of oxazine rings. The small peaks around 280 °C for poly(*o*-AB-fbz), poly(*o*-AF-fbz), and poly(*o*-AP-fbz) were attributed to the rearrangement of polybenzoxazine into polybenzoxazole according to published work.[55]

FT-IR spectra were employed for further investigation of the curing procedures. In Figure 6b, the typical absorption band at 925 cm^{-1}, mainly standing for oxazine ring,[66] disappeared after the monomers was cured into polybenzoxazine. And the characteristic peak shown at 1362 cm^{-1} (CH_2 wagging into the closed benzoxazine ring) was also disappeared after curing reaction. As for the band at 1595 cm^{-1}, indicating the formation of polybenzoxazole structure, was not observed, which proved that the rearrangement of poly(*o*-AB-fbz), poly(*o*-AF-fbz) and poly(*o*-AP-fbz) during the curing reaction was inhibited. The typical absorption bonds for benzoxazine

DOI: 10.1021/acs.macromol.8b00741
Macromolecules XXXX, XXX, XXX−XXX

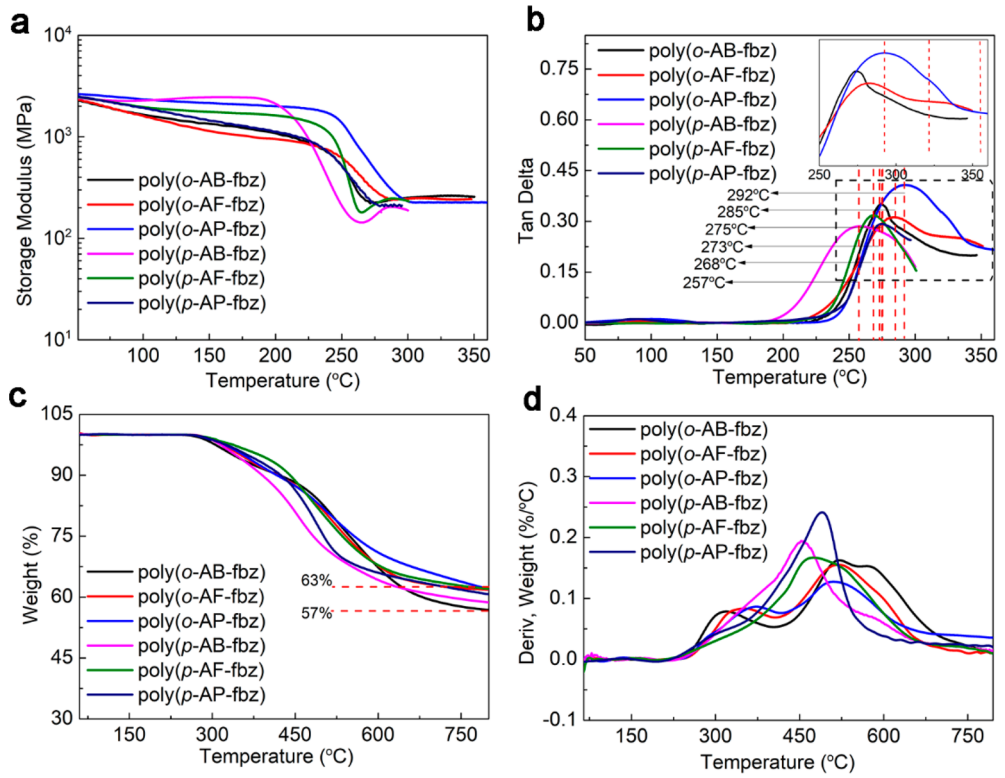

Figure 7. DMA curves of cured systems: (a) storage modulus as a function of temperature and (b) tan δ as a function of temperature for the different cured resins; TGA curves (c) and differential curves (d) for the cured systems under N_2.

Table 2. Mechanical and Thermal Properties for the Different Cured Systems

samples	T_g (°C)	storage modulus at T_g + 30 K (MPa)	cross-link density (mol dm^{-3})	$T_{d5\%}$ (°C)	T_{max} (°C)	char yield at 800 °C (%)
poly(*o*-AB-fbz)	275	233	16.1	338	542	57
poly(*o*-AF-fbz)	285	229	15.6	351	537	62
poly(*o*-AP-fbz)	292	221	15.2	354	532	62
poly(*p*-AB-fbz)	257	204	14.6	347	450	59
poly(*p*-AF-fbz)	268	223	15.7	370	507	63
poly(*p*-AP-fbz)	273	210	14.6	364	482	61

ring in *p*-AB-fbz, *p*-AF-fbz, and *p*-AP-fbz were presented at 928 and 1363 cm^{-1}. And their disappearance after curing reaction suggested the formation of poly(*p*-AB-fbz), poly(*p*-AF-fbz), and poly(*p*-AP-fbz) again. Combined with the results from DSC and FT-IR, the report concluded that all of the model benzoxazine precursors were cured completely, following the programmed temperature rising method, and more important, the rearrangement reaction was inhibited successfully.

The Thermal Performance of Polybenzoxazines. DMA was taken to investigate the dynamic mechanical properties of cured systems. Figure 7a shows the storage modulus, E', of poly(*o*-AB-fbz), poly(*o*-AF-fbz), poly(*o*-AP-fbz), poly(*p*-AB-fbz), poly(*p*-AF-fbz), and poly(*p*-AP-fbz) as a function of temperature, respectively. The E' of cured polybenzoxazines was in the range 2.6−2.9 GPa at room temperature and no significant differences were noticed. Conventionally, T_g of cured samples was determined by the peak temperature in the tan δ *vs* temperature graph (Figure 7(b)). And poly(*o*-AB-fbz), poly(*o*-AF-fbz), poly(*o*-AP-fbz), poly(*p*-AB-fbz), poly(*p*-AF-fbz), and poly(*p*-AP-fbz) showed T_g in the sequence 275, 285, 292, 257, 268, and 273 °C. Obviously, the T_g of cured polybenzoxazines containing different bridging units (benzene, furan, and pyridine) followed the order poly(*o*-AB-fbz) < poly(*o*-AF-fbz) < poly(*o*-AP-fbz) and poly(*p*-AB-fbz) < poly(*p*-AF-fbz) < poly(*p*-AP-fbz). In addition, compared with the literature results,[59,67−70] these polybenzoxazines showed higher T_g relative to the polybenzoxazines derived from bisphenol A, whose T_g was usually about 180 °C.

As we know, the thermal properties of polybenzoxazines will be greatly affected by their cross-link density, which is defined as the number of moles of network chains per volume unit of the cured material.[7,71] And the rubber elasticity theory is usually applied for the determination of thermosets' cross-link density. According to this theory, the storage modulus in the rubbery plateau (E'_R) will change with the cross-link density and it can be calculated by the following eq 3:

$$\vartheta_c = \frac{E'_R}{3RT} \tag{3}$$

where ϑ_c was the cross-link density (mol dm^{-3}), E'_R was the plateau modulus in the rubbery state (Pa), which was read at T_g + 30 K, R was the gas constant (J mol^{-1} g^{-1}), and T was the absolute temperature at T_g + 30 K. The thus calculated ϑ_c values for all the cured systems were listed in Table 2. It was noted that all the polybenzoxazines showed similar cross-link

DOI: 10.1021/acs.macromol.8b00741
Macromolecules XXXX, XXX, XXX−XXX

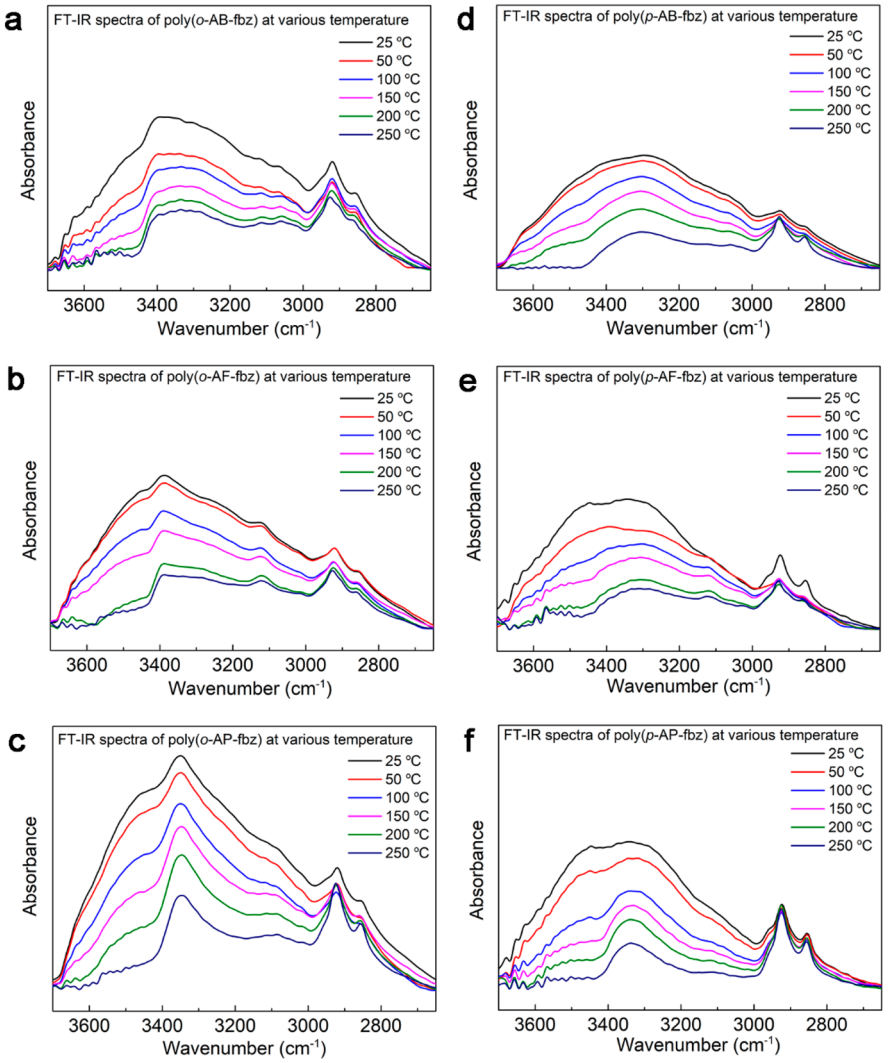

Figure 8. Normalized FT-IR spectra of all the cured different systems at various temperatures (25, 50, 100, 150, 200, and 250 °C): (a) poly(*o*-AB-fbz), (b) poly(*o*-AF-fbz), (c) poly(*o*-AP-fbz), (d) poly(*p*-AB-fbz), (e) poly(*p*-AF-fbz), and (f) poly(*p*-AP-fbz).

density, which indicated that the difference in T_g was not caused by the cross-link density.

Considering the similar structures of synthesized model monomers and literature results,[72−74] the different T_g of the cured polybenzoxazines was possibly caused by the formation and varied strength of H-bonding, which would be clearly analyzed and explained in the following part. What should be mentioned here was that the tan δ of poly(*o*-AB-fbz), poly(*o*-AF-fbz) or poly(*o*-AP-fbz) did not show a dramatic decrease after the peak temperature with a indistinct broad peak, presented in Figure 7b. It might be caused by the cyclodehydration of *o*-amide-functionalized polybenzoxazine above T_g, after which the polybenzoxazine was converted into polybenzoxazole. These results were consistent with the DSC heating curves in Figure 6a, which were also reported in Ishida's work.[55]

The thermal stability of the cured system was investigated by TGA under nitrogen (Figure 7(c)) and the related data was listed in Table 2. The temperature of 5% weight loss ($T_{d5\%}$) was 338 °C for poly(*o*-AB-fbz), 351 °C for poly(*o*-AF-fbz), 354 °C for poly(*o*-AP-fbz), 347 °C for poly(*p*-AB-fbz), 370 °C for poly(*p*-AF-fbz), and 364 °C for poly(*p*-AP-fbz). In general, the $T_{d5\%}$ values of polybenzoxazines with *p*-amide structure were higher than those of *o*-amide substituted analogues. As for the fastest degradation temperature (T_{max}), T_{max} of poly(*p*-AB-fbz), poly(*p*-AF-fbz), and poly(*p*-AP-fbz) was in turn 457, 473, and 488 °C. However, the T_{max} of poly(*o*-AB-fbz), poly(*o*-AF-fbz) and poly(*o*-AP-fbz) was high up to 542, 537, and 532 °C, respectively, which was much higher than those of the analogues with *para*-substituted amide group. This phenomenon was related to the fact that there were two peaks in the differential TGA curves of poly(*o*-AB-fbz), poly(*o*-AF-fbz), and poly(*o*-AP-fbz) (Figure 7d), while only one peak was observed in the differential curves of poly(*p*-AB-fbz), poly(*p*-AF-fbz), and poly(*p*-AP-fbz). These results confirmed the conversion of *o*-amide functionalized polybenzoxazines to polybenzoxazole again, which was accompanied by the release of water. In the Supporting Information, the conversion reaction was clearly identified with the help of DSC, FT-IR and TGA (Figure S21). As far as the char yield was concerned, it was as high as 57 wt % for poly(*o*-AB-fbz), 62 wt % for poly(*o*-AF-fbz), 62 wt % for poly(*o*-AP-fbz), 59 wt % for poly(*p*-AB-fbz), 63 wt % for poly(*p*-AF-fbz), and 61 wt % for poly(*p*-AP-fbz) at 800 °C. These results were normal.

FT-IR Spectra Analysis for the Cured Systems. As mentioned above, the high T_g of polybenzoxazines in this work

DOI: 10.1021/acs.macromol.8b00741
Macromolecules XXXX, XXX, XXX−XXX

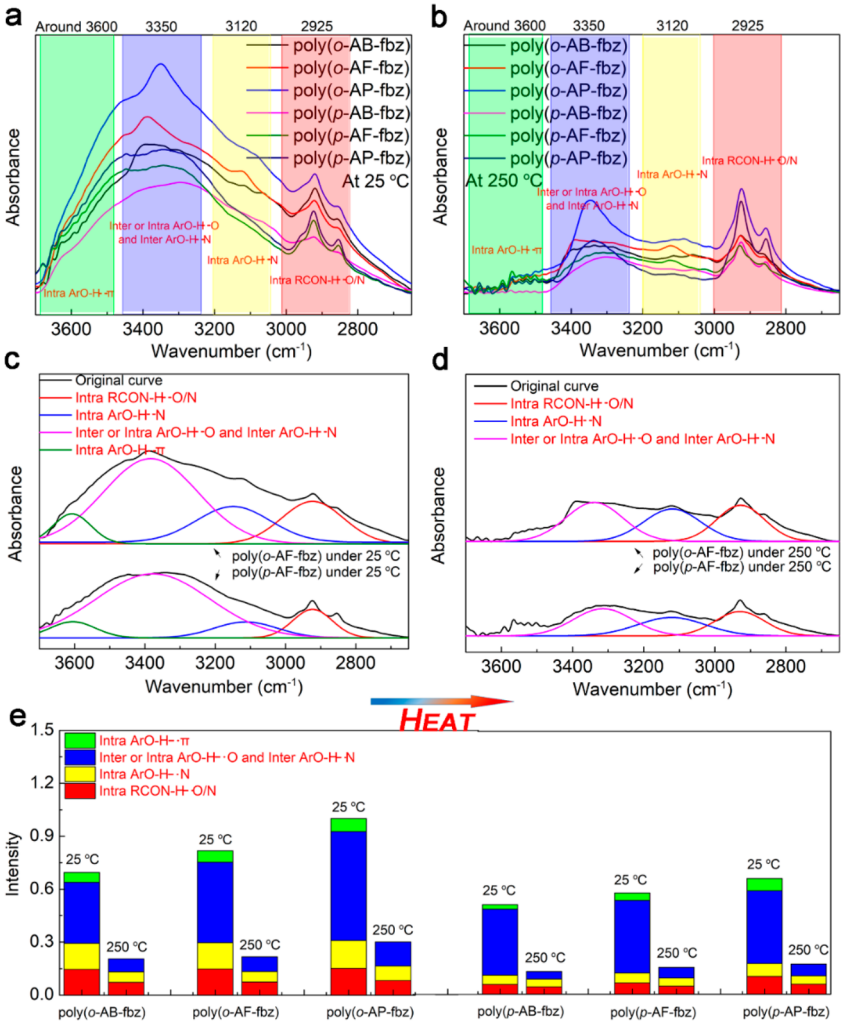

Figure 9. Different types of hydrogen bonding in all the cured systems depicted in FT-IR spectra at 25 (a) and 250 °C (b) after normalization; splitting FT-IR spectra between 2650 and 3700 cm^{-1} of poly(*o*-AF-fbz) and poly(*p*-AF-fbz) under 25 (c) or 250 °C (d); (e) comparison of split peaks' integrated areas in different systems at 25 and 250 °C.

was possibly related to the formation of H-bonding and their difference was caused by the varied H-bonding strength. Normalized FT-IR spectra were used to investigate the H-bonding interactions in all the cured systems at various temperatures (25, 50, 100, 150, 200, and 250 °C) (Figure 8). As we know, the intramolecular H-bonding -O$^-$--H$^+$N−, −OH--N−, −OH--O− and −OH--π usually show the characteristic absorption bonds at ∼2900, ∼ 3180, ∼ 3460 and ∼3550 cm^{-1}, respectively. The intermolecular H-bonding −OH--N− and −OH--O− can be identified by the typical absorption bands at ∼3300 and ∼3380 cm^{-1}. And the peaks above 3600 cm^{-1} refer to the free − OH and intermolecular −OH--π.[39,40,75,76] In order to clearly study the features of H-bonding in the cured systems, only the absorption peaks between 2650 and 3700 cm^{-1} were shown. In Figure 8a−f, it was noted that the typical absorption bonds for H-bonding was gradually deceased when the temperature was increased from 25 to 250 °C and the still presence of H-bonding interactions in poly(*o*-AB-fbz, poly(*o*-AF-fbz), poly(*o*-AP-fbz), poly(*p*-AB-fbz), poly(*p*-AF-fbz), and poly(*p*-AP-fbz) at 250 °C was supported by the obvious characteristic absorption bonds. This result meant that it was reasonable for us to attribute the relatively higher T_g to the formation of H-bonding even at 250 °C, which hindered the motion of molecular segments and then led to a higher T_g. However, what type of H-bonding, intermolecular or intramolecular ("In the same or different chain/unit" might be more accurate in the cross-linked systems. However, considering the expression custom, "intermolecular or intramolecular" was still employed here for the cured resins), tend to exist at higher temperature and how would the chemical structure (different bridging units: benzene, furan and pyridine) influence the formation of inter- or intramolecular H-bonding in the cured resins, were remained to be answered in the following part.

Figure 9 showed the FT-IR spectra comparison between all the cured systems at 25 (Figure 9a) and 250 °C (Figure 9b). On the basis of the chemical structures of cured systems, the characteristic bonds showing at 2925 cm^{-1} were assigned to the intramolecular H-bonding RCON−H--N (pyridine) and RCON−H--O (furan or Ar). While the peaks centered at 3120 cm^{-1} were corresponding to the intramolecular H-bonding of ArO−H--N (pyridine or N atom in other groups), peaks around 3350 cm^{-1} were standing for the inter- or intramolecular H-bonding ArOH--O (carbonyl, furan or Ar) and intermolecular H-bonding ArOH--N, peaks showing at 3600 cm^{-1} were attributed to the intramolecular H-bonding −OH--

DOI: 10.1021/acs.macromol.8b00741
Macromolecules XXXX, XXX, XXX−XXX

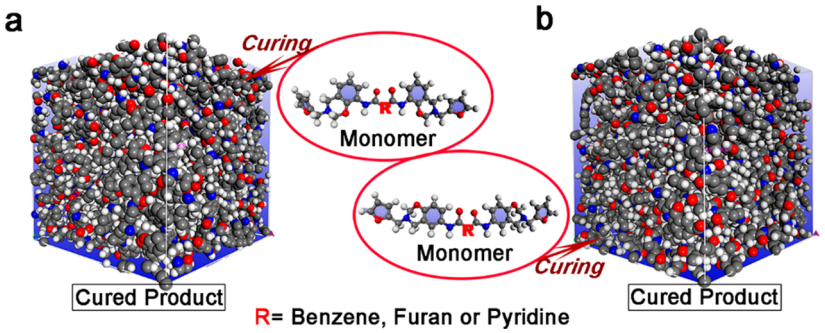

Figure 10. Molecular structures of cross-linked polybenzoxazines: (a) for poly(*o*-AB-fbz), poly(*o*-AF-fbz), and poly(*o*-AP-fbz) and (b) for poly(*p*-AB-fbz), poly(*p*-AF-fbz), and poly(*p*-AP-fbz).

Table 3. Simulation Properties for Cross-Linked Polybenzoxazines

samples	poly(*o*-AB-fbz)	poly(*o*-AF-fbz)	poly(*o*-AP-fbz)	poly(*p*-AB-fbz)	poly(*p*-AF-fbz)	poly(*p*-AP-fbz)
density @ 300 K (g/cm^3)	1.13	1.15	1.15	1.13	1.13	1.13
T_g (°C)	267	277	289	240	252	265
H-bonding density (10^{-3} mol/cm^3)	3.59 ± 0.11	3.98 ± 0.12	4.04 ± 0.08	3.19 ± 0.08	3.43 ± 0.11	3.49 ± 0.09

π (benzene, furan or pyridine) and free −OH. It was noted that, in general, the intensity of all the absorption bonds between 2650 and 3700 cm^{-1} was in accordance with the following order: poly(*o*-AP-fbz) > poly(*o*-AF-fbz) > poly(*o*-AB-fbz) > poly(*p*-AP-fbz) > poly(*p*-AF-fbz) > poly(*p*-AB-fbz), both at 25 and 250 °C, which roughly agreed with the order of their T_g. In order to obtain deeper information, the FT-IR spectra were analyzed by means of overlapping peak resolving (keeping the characteristic frequency at 2925, 3120, 3350, and 3600 cm^{-1}, where all of the R^2 values of the fitting curves are above 0.9). For conciseness, only the split spectra of poly(*o*-AF-fbz) and poly(*p*-AF-fbz) under 25 (Figure 9c) and 250 °C (Figure 9d) were shown here and the others were put in the Supporting Information (Figures S22−S29). According to the peak assignment, the FT-IR spectra at 25 °C was split into four peaks, respectively centered at 2925, 3120, 3350, and 3600 cm^{-1}, and the spectra at 250 °C were divided into three parts (2925, 3120, and 3350 cm^{-1}) due to the disappearance of absorption at 3600 cm^{-1}. It was easy to notice that the intensity of split peaks were varied in the different systems and their integrated areas were taken to qualitatively compare the strength of different H-bonding interactions. The integrated areas of all the split peaks in different systems were obtained and their ratios were demonstrated in Figure 9e. At 25 °C, the inter- and intramolecular H-bonding ArOH--O (carbonyl, furan or Ar) and intermolecular H-bonding ArOH--N were predominant in all the cured systems. Compared with the *p*-amide-substituted systems, not only the strength of H-bonding in poly(*o*-AP-fbz), poly(*o*-AF-fbz) and poly(*o*-AB-fbz), but also the percentage of intramolecular H-bonding, such as RCON−H--N (pyridine), RCON−H--O (furan or Ar), ArOH--N (pyridine or other groups), and ArOH--O (carbonyl), were relatively higher. When the temperature was increased up to 250 °C, the intensity of absorption bonds in all the systems were dramatically decreased, especially the ones standing for the intermolecular H-bonding, although the IR extinction coefficient of even the same band will change at different temperature, which will influence the intensity of the absorption bonds. The temperature-dependent IR is usually employed to semiquantitatively compare the strength of H-bonding, considering the slight change of extinction coefficient at different temperature. In this work, the decreased intensity of absorption bonds at higher temperature should be related with the decreased H-bonding strength. And this was easy to understand because the strength of intramolecular H-bond was usually stronger than the interaction between different molecules, and the higher temperature would easily destroy weaker H-bonding, then led to the increased ratio of intramolecular ones. As mentioned above, the bridging units in different benzoaxzines, benzene, furan, and pyridine demonstrated different electron-donating abilities, which could influence the formation and strength of H-bonding in the cured resins. The pyridine units showed the strongest ability to attract protons and was followed by the furan units. Therefore, the density or strength of H-bonding in the *o*-amide-functionalized systems should follow the order poly(*o*-AP-fbz) > poly(*o*-AF-fbz) > poly(*o*-AB-fbz). This speculation was supported by the H-bonding strength comparison in Figure 9e and in line with the order of their T_g. As for the *p*-amide substituted systems, their T_g followed the order of poly(*p*-AP-fbz) > poly(*p*-AF-fbz) > poly(*p*-AB-fbz). And the reason was also related to the H-bonding strength. In addition, compared to the strength of intramolecular H-bonding with the intermolecular interaction at 25 and 250 °C, the intramolecular H-bonding was undoubtedly playing a more important role in affecting the T_g of cured resins, due to the lower stability of intramolecular hydrogen bonds at high temperature. On the basis of these results, the conclusion might be drawn that there was a close positive correlation between the H-bonding interactions, especially the intramolecular ones, and thermal property (T_g) of polybenzoxazines.

MD Simulation for the Model Systems. After the multistep cross-linking reaction and topology relaxation via MD simulation, the final structures of polybenzoxazines were shown in Figure 10. The density at room temperature (300 K) was 1.13, 1.15, 1.15, 1.13, 1.13, and 1.13 g cm^{-3} for poly(*o*-AB-fbz), poly(*o*-AF-fbz), poly(*o*-AP-fbz), poly(*p*-AB-fbz), poly(*p*-AF-fbz), and poly(*p*-AP-fbz), respectively. And the relevant data is summarized in Table 3.

The well-relaxed network of each polybenzoxazine system was obtained after being experienced an equilibration at 850 K

DOI: 10.1021/acs.macromol.8b00741
Macromolecules XXXX, XXX, XXX−XXX

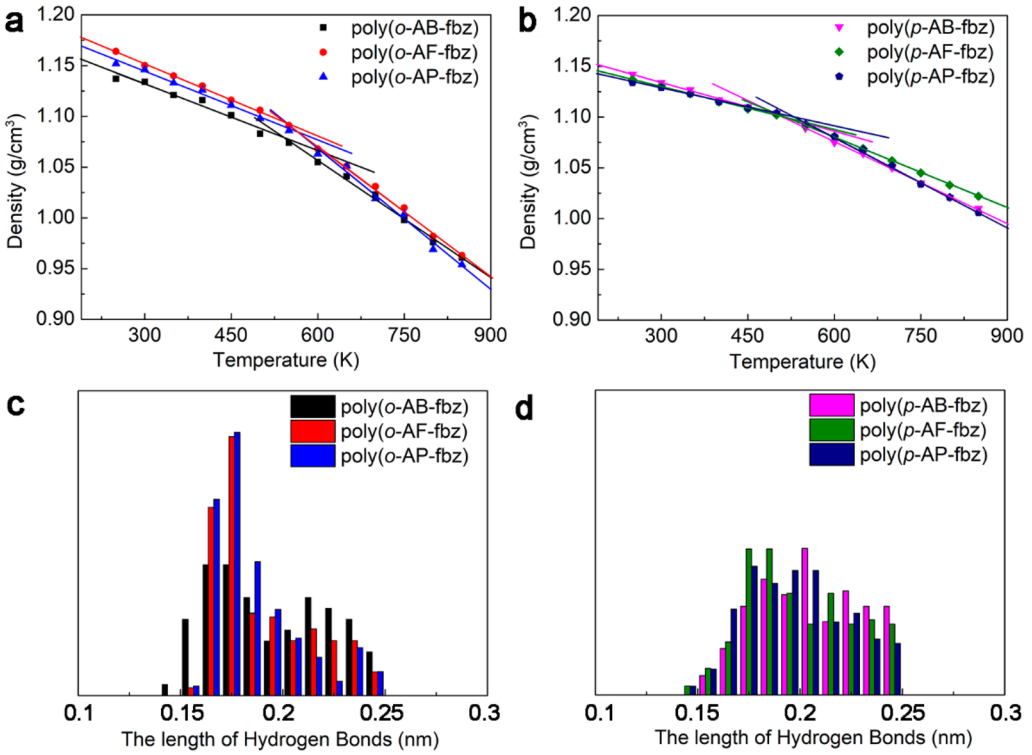

Figure 11. Temperature dependence of density for polybenzoxazines (a, b) and the H-bonding length distribution (c) for poly(*o*-AB-fbz), poly(*o*-AF-fbz), and poly(*o*-AP-fbz) and (d) for poly(*p*-AB-fbz), poly(*p*-AF-fbz), and poly(*p*-AP-fbz).

in NPT, followed by an annealing simulation, i.e. a cooling down process at the rate of 50 K/200 ps to 250 K using *NPT*-MD simulations. According to the results from the annealing simulation, the dependence of density on the temperature for each cross-linked system was shown in Figure 11, parts a and b. The characteristic turning points in the slope of the density−temperature curve was observed, where the temperature was corresponding to T_g. In order to get the exact values of T_g, linear fit with more than 98% confidence was performed and the thus obtained T_gs were listed in Table 3. As shown in Table 3, the calculated T_gs for the cross-linked systems were 267 °C for poly(*o*-AB-fbz), 277 °C for poly(*o*-AF-fbz), 289 °C for poly(*o*-AP-fbz), and 240 °C for poly(*p*-AB-fbz), 252 °C for poly(*p*-AF-fbz), 265 °C for poly(*p*-AP-fbz), respectively, which were all a light lower than the experimentally observed T_gs (275 °C for poly(*o*-AB-fbz), 285 °C for poly(*o*-AF-fbz), 292 °C for poly(*o*-AP-fbz), and 257 °C for poly(*p*-AB-fbz), 268 °C for poly(*p*-AF-fbz), 273 °C for poly(*p*-AP-fbz) based on above DMA measurement). The reason might be that the molecular dynamic simulation was conducted only based on the oxazine ring polymerization mechanism disregarding the possible furfuryl group polymerization. Actually, the furfuryl group would participate in the polymerization in various mechanisms, which led to the elevated T_gs.

As defined by Kim and Mattice,[52] a H-bonding formed when the distance between a donor −OH and an acceptor -O or -N was less than 0.25 nm and the angle of − O−H−O− or − O−H−N was in the range of 120° to 180°. In this work, the values of H-bonding density were averaged over five frames in the last 100 ps during the MD simulations. From Table 3, it was noted that the calculated H-bonding density was related to the values of T_g. The higher the H-bonding density, the higher the T_g. As a matter of fact, not only the quantity, but also the strength of each bond influence the overall strength of H-bonding. And H-bonding strength is related to the bond length. Therefore, the distribution of H-bonds length for all the cross-linked polybenzoxazine was summarized and represented in Figure 11, parts c and d. In comparison of the systems containing *o*-amide groups (poly(*o*-AB-fbz), poly(*o*-AF-fbz), and poly(*o*-AP-fbz)) with the *para*-amide functionalized systems (poly(*p*-AB-fbz), poly(*p*-AF-fbz), and poly(*p*-AP-fbz)), more hydrogen bonds with the length less than 0.2 nm were observed in the former systems, indicating their higher hydrogen bond strength. As for poly(*o*-AB-fbz), poly(*o*-AF-fbz), and poly(*o*-AP-fbz), the content of hydrogen bonds showing the bond length in the range of 0.15 to 0.2 nm followed the order of poly(*o*-AB-fbz) < poly(*o*-AF-fbz) < poly(*o*-AP-fbz). This was same as the sequence of their T_gs, either obtained from DSC measurement or MD simulation. In Figure 11d, it could note that the statistical length of hydrogen bonds in poly(*p*-AP-fbz) was shorter than those in poly(*p*-AB-fbz) and poly(*p*-AF-fbz), although the length distribution of hydrogen bonds was more even compared with that in Figure 11c. On the basis of these results, it could conclude that both the overall H-bonding strength and T_g obtained from MD simulation followed the order of poly(*o*-AB-fbz) < poly(*o*-AF-fbz) < poly(*o*-AP-fbz) and poly(*p*-AB-fbz) < poly(*p*-AF-fbz) < poly(*p*-AP-fbz), which was same as the experimental results and verified the conclusion based on experiments.

CONCLUSION

The model benzoxazine monomers *o*-AB-fbz, *o*-AF-fbz, *o*-AP-fbz, *p*-AB-fbz, *p*-AF-fbz, and *p*-AP-fbz were carefully designed and successfully synthesized. It was found that not only the formation but also the type and strength of H-bonding played a significant role in determining the curing behaviors of benzoxazines. It was the H-bonding involved with the oxygen atom in oxazine ring, rather than all of the H-bonding, that

DOI: 10.1021/acs.macromol.8b00741
Macromolecules XXXX, XXX, XXX−XXX

accelerated the curing reactions, and the higher strength will lead to higher reactivity. Different from the curing reaction, it was the overall H-bonding interactions that were important, including all the inter- and intramolecular ones, and their strengths were positively correlated with the T_g of polybenzoxazines based on the FT-IR analysis. However, the intramolecular H-bonding played a more important role in affecting the T_g, due to their higher stabilities at high temperature. It was the first time that not only the formation of H-bonding but also their type and strength in benzoxazine monomers and the cured products were characterized and qualitatively investigated. Their roles in affecting the curing behaviors of benzoxazine and thermal properties of cured polybenzoxazines were studied in detail. The information provided in this paper could help us understand polybenzoxazines more deeply and manipulate their properties efficiently.

■ ASSOCIATED CONTENT

Supporting Information

The Supporting Information is available free of charge on the ACS Publications website at DOI: 10.1021/acs.macromol.8b00741.

NMR spectra of compounds **1**−**6**, *o*-AB-fbz, *o*-AF-fbz, *o*-AP-fbz, *p*-AB-fbz, *p*-AF-fbz, and *p*-AP-fbz; mass spectra of *o*-AB-fbz, *o*-AF-fbz, *o*-AP-fbz, *p*-AB-fbz, *p*-AF-fbz, and *p*-AP-fbz; and splitting FT-IR spectra for poly(*o*-AB-fbz), poly(*o*-AF-fbz), poly(*o*-AP-fbz), poly(*p*-AB-fbz), poly(*p*-AF-fbz), and poly(*p*-AP-fbz) at 25 and 250 °C, respectively (PDF)

■ AUTHOR INFORMATION

Corresponding Author

*Address: 1219 Zhongguan West Rd., Zhenhai District, Ningbo 315201, China. E-mail: liuxq@nimte.ac.cn. (X.L.).

ORCID

Xiaoqing Liu: 0000-0002-7417-1326

Shiyu Du: 0000-0001-6707-3915

Author Contributions

#This author made an equal contribution to the first author.

Notes

The authors declare no competing financial interest.

■ ACKNOWLEDGMENTS

The authors greatly thank the National Key Technology Support Program (2015BAD15B08), the National Key Research and Development Program of China (2018YFD0400700), the National Natural Science Foundation of China (NSFC 51373194; NSFC 51503217), the Chinese Academy of Sciences (Key Research Program ZDRW-CN-2016-1), the Research Project of Technology Application for Public Welfare of Zhejiang Province (2017C31081), and the Ningbo Natural Science Foundation (No. 2017A610053) for financial support.

■ REFERENCES

(1) Ishida, H. *Handbook of Benzoxazine Resins* **2011**, 3−81.

(2) Ghosh, N. N.; Kiskan, B.; Yagci, Y. Polybenzoxazines-New High Performance Thermosetting Resins: Synthesis and Properties. *Prog. Polym. Sci.* **2007**, *32*, 1344−1391.

(3) Nair, C. P. R. Advances in Addition-Cure Phenolic Resins. *Prog. Polym. Sci.* **2004**, *29*, 401−498.

(4) Takeichi, T.; Kawauchi, T.; Agag, T. High Performance Polybenzoxazines as a Novel Type of Phenolic Resin. *Polym. J.* **2008**, *40*, 1121−1131.

(5) Holly, F. W.; Cope, A. C. Condensation Product of Aldehydes and Ketones with o-Aminobenzyl Alcohol and o-Hydroxybenzylamine. *J. Am. Chem. Soc.* **1944**, *66*, 1875−1879.

(6) Ning, X.; Ishida, H. Phenolic Materials via Ring-Opening Polymerization-Synthesis and Characterization of Bisphenol-A Based Benzoxazines and Their Polymers. *J. Polym. Sci., Part A: Polym. Chem.* **1994**, *32*, 1121−1129.

(7) Ishida, H.; Allen, D. J. Mechanical Characterization of Copolymers Based on Benzoxazine and Epoxy. *Polymer* **1996**, *37*, 4487−4495.

(8) Takeichi, T.; Saito, Y.; Agag, T.; Muto, H.; Kawauchi, T. High-Performance Polymer Alloys of Polybenzoxazine and Bismaleimide. *Polymer* **2008**, *49*, 1173−1179.

(9) Takeichi, T.; Guo, Y.; Agag, T. Synthesis and Characterization of Poly(urethane-benzoxazine) Films as Novel Type of Polyurethane/Phenolic Resin Composites. *J. Polym. Sci., Part A: Polym. Chem.* **2000**, *38*, 4165−4176.

(10) Wang, M. W.; Jeng, R. J.; Lin, C. H. Origin of The Rapid Trimerization of Cyanate Ester in a Benzoxazine/Cyanate Ester Blend. *Macromolecules* **2015**, *48*, 2417−2421.

(11) Li, X. D.; Gu, Y. The Co-Curing Process of a Benzoxazine-Cyanate System and The Thermal Properties of The Copolymers. *Polym. Chem.* **2011**, *2*, 2778−2781.

(12) Ishida, H.; Chaisuwan, T. Mechanical Property Improvement of Carbon Fiber Reinforced Polybenzoxazine by Rubber Interlayer. *Polym. Compos.* **2003**, *24*, 597−607.

(13) Zeng, M.; Wang, J.; Li, R. R.; Liu, J. X.; Chen, W.; Xu, Q. Y.; Gu, Y. The Curing Behavior and Thermal Property of Graphene Oxide/Benzoxazine Nanocomposites. *Polymer* **2013**, *54*, 3107−3116.

(14) Santhosh Kumar, K. S.; Reghunadhan Nair, C. P.; Ninan, K. N. Silica Fiber-Polybenzoxazine-Syntactic Foams; Processing and Properties. *J. Appl. Polym. Sci.* **2008**, *107*, 1091−1099.

(15) Ishida, H.; Low, H. Y. Synthesis of Benzoxazine Functional Silane and Adhesion Properties of Glass-Fiber-Reinforced Polybenzoxazine Composites. *J. Appl. Polym. Sci.* **1998**, *69*, 2559−2567.

(16) Yang, C. C.; Lin, Y. C.; Wang, P. I.; Liaw, D. J.; Kuo, S. W. Polybenzoxazine/Single-Walled Carbon Nanotube Nanocomposites Stabilized Through Noncovalent Bonding Interactions. *Polymer* **2014**, *55*, 2044−2050.

(17) Agag, T.; Takeichi, T. Synthesis, Characterization and Clay-Reinforcement of Epoxy Cured with Benzoxazine. *High Perform. Polym.* **2002**, *14*, 115−132.

(18) Agag, T.; Takeichi, T. Preparation and Cure Behavior of Organoclay-Modified Allyl-Functional Benzoxazine Resin and The Properties of Their Nanocomposites. *Polym. Compos.* **2008**, *29*, 750−757.

(19) Andreu, R.; Reina, J. A.; Ronda, J. C. Carboxylic Acid-Containing Benzoxazines as Efficient Catalysts in The Thermal Polymerization of Benzoxazines. *J. Polym. Sci., Part A: Polym. Chem.* **2008**, *46*, 6091−6101.

(20) Agag, T.; Takeichi, T. Novel Benzoxazine Monomers Containing p-Phenyl Propargyl Ether: Polymerization of Monomers and Properties of Polybenzoxazines. *Macromolecules* **2001**, *34*, 7257−7263.

(21) Zhang, K.; Liu, J.; Ishida, H. An Ultrahigh Performance Cross-Linked Polybenzoxazole via Thermal Conversion from Poly(benzoxazine amic acid) Based on Smart o-Benzoxazine Chemistry. *Macromolecules* **2014**, *47*, 8674−8681.

(22) Zhang, K.; Ishida, H. An Anomalous Trade-Off Effect on The Properties of Smart ortho-Functional Benzoxazines. *Polym. Chem.* **2015**, *6*, 2541−2550.

(23) Zhang, K.; Han, L.; Froimowicz, P.; Ishida, H. A Smart Latent Catalyst Containing o-Trifluoroacetamide Functional Benzoxazine: Precursor for Low Temperature Formation of Very High Performance Polybenzoxazole with Low Dielectric Constant and High Thermal Stability. *Macromolecules* **2017**, *50*, 6552−6560.

DOI: 10.1021/acs.macromol.8b00741
Macromolecules XXXX, XXX, XXX−XXX

(24) Hanbeyoglu, B.; Kiskan, B.; Yagci, Y. Hydroxyl Functional Polybenzoxazine Precursor as A Versatile Platform for Post-Polymer Modifications. *Macromolecules* **2013**, *46*, 8434−8440.
(25) Agag, T.; Geiger, S.; Alhassan, S. M.; Qutubuddin, S.; Ishida, H. Low-Viscosity Polyether-Based Main-Chain Benzoxazine Polymers: Precursors for Flexible Thermosetting Polymers. *Macromolecules* **2010**, *43*, 7122−7127.
(26) Kudoh, R.; Sudo, A.; Endo, T. Synthesis of Eight-Membered Lactone Having Tertiary Amine Moiety by Ring-Expansion Reaction of 1,3-Benzoxazine and Its Anionic Ring-Opening Polymerization Behavior. *Macromolecules* **2009**, *42*, 2327−2329.
(27) Froimowicz, P.; Zhang, K.; Ishida, H. Intramolecular Hydrogen Bonding in Benzoxazines: When Structural Design Becomes Functional. *Chem. - Eur. J.* **2016**, *22*, 2691−2707.
(28) Baqar, M.; Agag, T.; Huang, R. Z.; Maia, J.; Qutubuddin, S.; Ishida, H. Mechanistic Pathways for The Polymerization of Methylol-Functional Benzoxazine Monomers. *Macromolecules* **2012**, *45*, 8119−8125.
(29) Zhang, K.; Froimowicz, P.; Han, L.; Ishida, H. Hydrogen-Bonding Characteristics and Unique Ring-Opening Polymerization Behavior of Ortho-Methylol Functional Benzoxazine. *J. Polym. Sci., Part A: Polym. Chem.* **2016**, *54*, 3635−3642.
(30) Han, L.; Zhang, K.; Ishida, H.; Froimowicz, P. Study of The Effects of Intramolecular and Intermolecular Hydrogen-Bonding Systems on The Polymerization of Amide-Containing Benzoxazines. *Macromol. Chem. Phys.* **2017**, *218*, 1600562.
(31) Kolanadiyil, S. N.; Minami, M.; Endo, T. Synthesis and Thermal Properties of Difunctional Benzoxazines with Attached Oxazine Ring at the Para-, Meta-, and Ortho-Position. *Macromolecules* **2017**, *50*, 3476−3488.
(32) Arslan, M.; Kiskan, B.; Yagci, Y. Benzoxazine-Based Thermosets with Autonomous Self-Healing Ability. *Macromolecules* **2015**, *48*, 1329−1334.
(33) Taskin, O. S.; Kiskan, B.; Yagci, Y. Polybenzoxazine Precursors As Self-Healing Agents for Polysulfones. *Macromolecules* **2013**, *46*, 8773−8778.
(34) Alhwaige, A. A.; Agag, T.; Ishida, H.; Qutubuddin, S. Biobased Chitosan/Polybenzoxazine Cross-Linked Films: Preparation in Aqueous Media and Synergistic Improvements in Thermal and Mechanical Properties. *Biomacromolecules* **2013**, *14*, 1806−1815.
(35) Shen, X.; Dai, J.; Liu, Y.; Liu, X.; Zhu, J. Synthesis of High Performance Polybenzoxazine Networks from Bio-Based Furfurylamine: Furan vs Benzene Ring. *Polymer* **2017**, *122*, 258−269.
(36) Lin, C. H.; Chang, S. L.; Shen, T. Y.; Shih, Y. S.; Lin, H. T.; Wang, C. F. Flexible Polybenzoxazine Thermosets with High Glass Transition Temperatures and Low Surface Free Energies. *Polym. Chem.* **2012**, *3*, 935−945.
(37) Sini, N. K.; Endo, T. Toward Elucidating the Role of Number of Oxazine Rings and Intermediates in The Benzoxazine Backbone on Their Thermal Characteristics. *Macromolecules* **2016**, *49*, 8466−8478.
(38) Froimowicz, P.; Rodriguez Arza, C.; Ohashi, S.; Ishida, H. Tailor-Made and Chemically Designed Synthesis of Coumarin-Containing Benzoxazines and Their Reactivity Study Toward Their Thermosets. *J. Polym. Sci., Part A: Polym. Chem.* **2016**, *54*, 1428−1435.
(39) Kim, H. D.; Ishida, H. A Study on Hydrogen Bonding in Controlled-Structure Benzoxazine Model Oligomers. *Macromol. Symp.* **2003**, *195*, 123−146.
(40) Kim, H. D.; Ishida, H. A Study on Hydrogen-Bonded Network Structure of Polybenzoxazines. *J. Phys. Chem. A* **2002**, *106*, 3271−3280.
(41) Kim, H. D.; Ishida, H. Model Compounds Study on The Network Structure of Polybenzoxazines. *Macromolecules* **2003**, *36*, 8320−8329.
(42) Dolenský, B.; Konvalinka, R.; Jakubek, M.; Kral, V. Identification of Intramolecular Hydrogen Bonds as The Origin of Malfunctioning of Multitopic Receptors. *J. Mol. Struct.* **2013**, *1035*, 124−128.
(43) Che, P. H.; Lu, F.; Nie, X.; Huang, Y. Z.; Yang, Y. L.; Wang, F.; Xu, J. Hydrogen Bond Distinction and Activation Upon Catalytic Etherification of Hydroxyl Compounds. *Chem. Commun.* **2015**, *51*, 1077−1080.
(44) Wang, L. X.; Hu, B. Q.; Xiang, J. F.; Cui, J.; Hao, X.; Liang, T. L.; Tang, Y. L. N-Aryl-Substituted Anthranilamides with Intramolecular Hydrogen Bonds. *Tetrahedron* **2014**, *70*, 8588−8591.
(45) Pearson, A. J.; Panda, S. N-Prolinylanthranilamide Pseudopeptides as Bifunctional Organocatalysts for Asymmetric Aldol Reactions. *Org. Lett.* **2011**, *13*, 5548−5551.
(46) Yarovsky, I.; Evans, E. Computer Simulation of Structure and Properties of Crosslinked Polymers: Application to Epoxy Resins. *Polymer* **2002**, *43*, 963−969.
(47) Varshney, V.; Patnaik, S. S.; Roy, A. K.; Farmer, B. L. A Molecular Dynamics Study of Epoxy-Based Networks: Cross-linking Procedure and Prediction of Molecular and Material Properties. *Macromolecules* **2008**, *41*, 6837−6842.
(48) Li, C.; Strachan, A. Molecular Simulations of Crosslinking Process of Thermosetting Polymers. *Polymer* **2010**, *51*, 6058−6070.
(49) Li, C.; Strachan, A. Molecular Dynamics Predictions of Thermal and Mechanical Properties of Thermoset Polymer EPON862/DETDA. *Polymer* **2011**, *52*, 2920−2928.
(50) Masoumi, S.; Arab, B.; Valipour, H. A Study of Thermo-Mechanical Properties of The Cross-linked Epoxy: An Atomistic Simulation. *Polymer* **2015**, *70*, 351−360.
(51) Saiev, S.; Bonnaud, L.; Dubois, P.; Beljonne, D.; Lazzaroni, R. Modeling The Formation and Thermomechanical Properties of Polybenzoxazine Thermosets. *Polym. Chem.* **2017**, *8*, 5988−5999.
(52) Kim, W. K.; Mattice, W. L. A Fully Atomistic Model of An Amorphous Polybenzoxazine at Bulk Density. *Comput. Theor. Polym. Sci.* **1998**, *8*, 353−361.
(53) Kim, W. K.; Mattice, W. L. Static and Dynamic Behavior of H_2O and O_2 Penetrants in A Polybenzoxazine. *Macromolecules* **1998**, *31*, 9337−9344.
(54) Gomes, M.; Gandini, A.; Silvestre, A. J. D.; Reis, B. Synthesis and Characterization of Poly(2,5-furan dicarboxylate)s Based on A Variety of Diols. *J. Polym. Sci., Part A: Polym. Chem.* **2011**, *49*, 3759−3768.
(55) Agag, T.; Liu, J.; Graf, R.; Spiess, H. W.; Ishida, H. Benzoxazole Resin: A Novel Class of Thermoset Polymer via Smart Benzoxazine Resin. *Macromolecules* **2012**, *45*, 8991−8997.
(56) Mayo, S. L.; Olafson, B. D.; Goddard, W. A. Dreiding - A Generic Force-Field For Molecular Simulations. *J. Phys. Chem.* **1990**, *94*, 8897−8909.
(57) Gasteiger, J.; Marsili, M. Iterative Partial Equalization of Orbital Electronegativity - A Rapid Access to Atomic Charges. *Tetrahedron* **1980**, *36*, 3219−3228.
(58) Samoletov, A. A.; Dettmann, C. P.; Chaplain, M. A. J. Thermostats for "Slow" Configurational Modes. *J. Stat. Phys.* **2007**, *128*, 1321−1336.
(59) Froimowicz, P.; Paez, J. I.; Gerbino, L.; Ali, S. N.; Belgacem, M. N.; Gandini, A.; Strumia, M. C. Effect of The Molecular Structure on The Reactivity in A Family of Tetra-Amine Compounds Derived from Jeffamines. *Macromol. Res.* **2012**, *20*, 800−809.
(60) Zhang, W. F.; Froimowicz, P.; Arza, C. R.; Ohashi, S.; Xin, Z.; Ishida, H. Latent Catalyst-Containing Naphthoxazine: Synthesis and Effects on Ring-Opening Polymerization. *Macromolecules* **2016**, *49*, 7129−7140.
(61) Ishida, H.; Rodriguez, Y. Curing Kinetics of A New Benzoxazine-Based Phenolic Resin by Differential Scanning Calorimetry. *Polymer* **1995**, *36*, 3151−3158.
(62) Agag, T.; Arza, C. R.; Maurer, F. H. J.; Ishida, H. Primary Amine-Functional Benzoxazine Monomers and Their Use for Amide-Containing Monomeric Benzoxazines. *Macromolecules* **2010**, *43*, 2748−2758.
(63) Kissinger, H. E. Reaction Kinetics in Differential Thermal Analysis. *Anal. Chem.* **1957**, *29*, 1702−1706.
(64) Ozawa, T. A New Method of Analyzing Thermogravimetric Data. *Bull. Chem. Soc. Jpn.* **1965**, *38*, 1881−1886.

DOI: 10.1021/acs.macromol.8b00741
Macromolecules XXXX, XXX, XXX−XXX

(65) Liu, Y.; Wang, J.; Xu, S. Synthesis and Curing Kinetics of Cardanol-Based Curing Agents for Epoxy Resin by In Situ Depolymerization of Paraformaldehyde. *J. Polym. Sci., Part A: Polym. Chem.* **2014**, *52*, 472−480.
(66) Han, L.; Iguchi, D.; Gil, P.; Heyl, T. R.; Sedwick, V. M.; Arza, C. R.; Ohashi, S.; Lacks, D. J.; Ishida, H. Oxazine Ring-Related Vibrational Modes of Benzoxazine Monomers Using Fully Aromatically Substituted, Deuterated, ^{15}N Isotope Exchanged, and Oxazine-Ring-Substituted Compounds and Theoretical Calculations. *J. Phys. Chem. A* **2017**, *121*, 6269−6282.
(67) Agag, T.; Jin, L.; Ishida, H. A New Synthetic Approach for Difficult Benzoxazines: Preparation and Polymerization of 4,4′-Diaminodiphenyl Sulfone-Based Benzoxazine Monomer. *Polymer* **2009**, *50*, 5940−5944.
(68) Zhang, K.; Liu, J.; Ohashi, S.; Liu, X. Y.; Han, Z. W.; Ishida, H. Synthesis of High Thermal Stability Polybenzoxazoles via Ortho-Imide-Functional Benzoxazine Monomers. *J. Polym. Sci., Part A: Polym. Chem.* **2015**, *53*, 1330−1338.
(69) Su, Y. C.; Chen, W. C.; Chang, F. C. Preparation and Characterization of Poly Seudorotaxanes Based on Adamantane-Modified Polybenzoxazines and Beta-Cyclodextrin. *Polymer* **2005**, *46*, 1617−1623.
(70) Wang, J.; Wu, M. Q.; Liu, W. B.; Yang, S. W.; Bai, J. W.; Ding, Q. Q.; Li, Y. Synthesis, Curing Behavior and Thermal Properties of Fluorene Containing Benzoxazines. *Eur. Polym. J.* **2010**, *46*, 1024−1031.
(71) Grishchuk, S.; Schmitt, S.; Vorster, O. C.; Karger-Kocsis, J. Structure and Properties of Amine-Hardened Epoxy/Benzoxazine Hybrids: Effect of Epoxy Resin Functionality. *J. Appl. Polym. Sci.* **2012**, *124*, 2824−2837.
(72) Liu, Y. L.; Chou, C. I. High Performance Benzoxazine Monomers and Polymers Containing Furan Groups. *J. Polym. Sci., Part A: Polym. Chem.* **2005**, *43*, 5267−5282.
(73) Hu, F. S.; La Scala, J. J.; Sadler, J. M.; Palmese, G. R. Synthesis and Characterization of Thermosetting Furan-Based Epoxy Systems. *Macromolecules* **2014**, *47*, 3332−3342.
(74) Shen, X. B.; Liu, X. Q.; Dai, J. Y.; Liu, Y.; Zhang, Y. J.; Zhu, J. How Does the Hydrogen Bonding Interaction Influence the Properties of Furan-Based Epoxy Resins. *Ind. Eng. Chem. Res.* **2017**, *56*, 10929−10938.
(75) Skrovanek, D. J.; Howe, S. E.; Painter, P. C.; Coleman, M. M. Hydrogen-Bonding in Polymers-Infrared Temperature Studies of An Amorphous Polyamide. *Macromolecules* **1985**, *18*, 1676−1683.
(76) Wu, Q. J.; Liu, X. H.; Berglund, L. A. FT-IR Spectroscopic Study of Hydrogen Bonding in PA6/Clay Nanocomposites. *Polymer* **2002**, *43*, 2445−2449.

DOI: 10.1021/acs.macromol.8b00741
Macromolecules XXXX, XXX, XXX−XXX